Chemical Geology 258 (2009) 5–16

Contents lists available at ScienceDirect

Chemical Geology

journal homepage: www.elsevier.com/locate/chemgeo

Lithium isotope analysis of olivine by SIMS: Calibration of a matrix effect and application to magmatic phenocrysts

David R. Bell [a,b,*], Richard L. Hervig [b], Peter R. Buseck [a,b], Sonja Aulbach [c,1]

[a] Department of Chemistry and Biochemistry, Arizona State University, Tempe AZ 85287, United States
[b] School of Earth and Space Exploration, Arizona State University, Tempe AZ 85287, United States
[c] Department of Geology, University of Maryland, College Park MD 20742, United States

ARTICLE INFO

Article history:
Accepted 3 October 2008

Keywords:
Mantle
Xenolith
Peridotite
Hawai'i
Ko'olau
Tanzania
South Africa
San Carlos
Kilbourne Hole
Geochemistry
Ion microprobe
Secondary ion mass spectrometry

ABSTRACT

High-spatial resolution analysis of light element isotope variations by secondary-ion mass spectrometry (SIMS) has numerous applications in geochemistry and cosmochemistry. Recent attention has focused on $^{7}Li/^{6}Li$ variations in magmatic phenocrysts to infer the volatile degassing history of their parent magmas, and on minerals from mantle samples to determine source-region processes and the recycling history of mantle reservoirs. In these studies the effect of mineral composition on the $^{7}Li/^{6}Li$ ratio measured by SIMS has been considered secondary, and generally disregarded. We show, using a suite of nine olivines analyzed by MC-ICP-MS or TIMS, that there is a substantial effect of composition on the $^{7}Li/^{6}Li$ ratio of olivine measured by SIMS. For magnesian olivine ($74<Fo<94$) the effect is a linear function of composition, with $\delta^{7}Li$ increasing by 1.3‰ for each mole percent decrease in forsterite component. At higher Fe contents, the relationship ceases to be linear. The composition range over which linear behavior is exhibited appears to depend on instrumental conditions. A calibration of this matrix effect over the linear range is presented, assuming the measurement of $^{7}Li/^{6}Li$ relative to an olivine standard of known composition. Application of this calibration to a suite of olivines separated from basaltic lavas from Ko'olau, Hawai'i demonstrates that the matrix effect is responsible for a geologically spurious correlation between $\delta^{7}Li$ and Mg#. However, after correction, the olivines retain evidence of Li isotope heterogeneity, the degree and nature of which differs in each of the four separates studied. These results emphasize the importance of compositional correction for SIMS measurement of $\delta^{7}Li$ in olivine, particularly in zoned crystals, and support previous conclusions that Li isotope variability in igneous materials is subject to late-stage disturbance. The significant matrix effect demonstrated for olivine suggests that matrix effects in other minerals require further evaluation.

1. Introduction

Secondary ion mass spectrometry (SIMS) analysis of micro-scale Li isotope and abundance variations in mineral grains plays an important role in establishing mechanisms and scales of isotope fractionation. The microanalyses permit assessment of intra-granular spatial correlations between concentration and isotopic profiles, and can be used to investigate diffusion-related concentration variations and isotopic fractionation, as well as other igneous processes such as volatile element degassing, magma mixing, or contamination. These SIMS analyses commonly traverse widely varying major element compositions of individual mineral grains (e.g., Beck et al., 2004). The effect of these varying matrix compositions on the instrumental capability to produce accurate Li isotope compositions has not been investigated systematically, but most studies conclude the effect to be negligible under the conditions investigated (Decitre et al., 2002; Beck et al., 2006).

A difference of ~4‰ was reported in the $\delta^{7}Li$ values obtained by SIMS for basaltic glasses depending on the use of olivines or clinopyroxene as a standard (Hervig et al., 2004). In that study, low energy secondary ions were collected (0±20 eV). Kasemann et al. (2005) noted a probable matrix effect for Li isotopes in siliceous glasses by observing a shift in instrumental mass fractionation (IMF) as a function of the degree of energy filtering applied to secondary ions, but they did not observe such a shift for basaltic glasses. The combined SIMS and MC-ICP-MS (multi-collector inductively coupled plasma mass spectrometry) study by Jeffcoate et al. (2007) noted possible matrix effects of a few ‰ in the analysis of olivines and pyroxenes from mantle xenoliths.

During an extensive program of Li isotope analyses of olivines from various mantle samples and meteorites, we observed a strong correlation between olivine composition (forsterite [Fo] content= Mg#=100 Mg/[Mg+Fe] on a molar basis) and $\delta^{7}Li$, prompting the systematic investigation of a possible matrix effect in this mineral. In this study we compare SIMS and MC-ICP-MS or thermal ionization mass spectrometry (TIMS) analyses of olivine samples with a range of

* Corresponding author. Department of Chemistry and Biochemistry, Arizona State University, Tempe AZ 85287, United States.
E-mail address: David.R.Bell@asu.edu (D.R. Bell).
[1] Present address: Department of Earth and Atmospheric Sciences, University of Alberta, Edmonton, Alberta, Canada T6G 2E3.

0009-2541/$ – see front matter © 2008 Elsevier B.V. All rights reserved.
doi:10.1016/j.chemgeo.2008.10.008

compositions to calibrate the effect of Mg# in olivine on the $^{7}Li/^{6}Li$ measured by SIMS. We then apply the calibration to a suite of olivine phenocrysts in basaltic lava (originally intended for use in the matrix calibration but found to be heterogeneous) to assess the degree of Li isotopic variability.

2. Samples

Sample details appear in Table 1. Most olivines used to calibrate the matrix effect were separated from peridotite xenoliths from Tanzania (89-773, LB29, LB51, LB59) and the SW USA (KBH-1, SC1-OL, SC-OL2). They include samples studied previously by Bell and Rossman, 1992; Rudnick et al., 1994; Seitz and Woodland, 2000; Seitz et al., 2004; Aulbach et al., 2008. Sample KPL-2 is a cumulate dunite xenolith from the 1800 Ka'upulehu Flow (Hualalai, Hawai'i). PMD99-149 is an Fe-rich olivine megacryst from the Gansfontein kimberlite, South Africa (Doyle, 1999). These samples range in composition from Fo74.1 to Fo93.6 and most are compositionally homogeneous. Minor heterogeneity in Fe/Mg was recorded in KPL-2 and LB51 (Table 1, Table A1). In KPL-2, two compositionally different groups of grains occur, and were treated as separate data points, although both were assigned the same bulk solution value for δ^{7}Li. In LB51 one grain had a different Fo content from other homogeneous grains and one grain was zoned. Consequently, the formal uncertainties that reflect this heterogeneity are greater for LB51 than for other samples. An additional sample of olivine with composition Fo52 is from a dunite from the Mooihoek pipe of the Bushveld Igneous Complex (Scoon and Mitchell, 2004). The grain sizes in these samples vary from ~2 mm to >1 cm.

A suite of phenocrysts separated from basalts of Ko'olau, Hawai'i was also analyzed in detail. These are grains remaining from the separates prepared and studied by Chan and Frey (2003) and are mostly in the size range of 0.5–1 mm. 68 analyses on 15 olivine grains drawn from four mineral separates were performed. A further 15 analyses were performed on four grains from separate KOO49, which subsequently proved to be either orthopyroxene or clinopyroxene. Originally, we planned to use both mantle olivines and the suite of olivines separated from Hawaiian basalts to calibrate the matrix effect.

During the study it became apparent that many of the separated phenocrysts (and a minor proportion of the mantle peridotite grains) showed variability in both Fo content and δ^{7}Li, rendering them less suitable as calibration standards than the more homogeneous mantle samples. Consequently, the matrix effect was calibrated using only the latter. After this matrix effect calibration was applied to the phenocrysts it was found that significant real variation in their Li isotopic composition exists. These variations are documented here and the implications for processes of Li isotope fractionation in basalts, and for the Li isotope analysis of such materials, are discussed.

3. Analytical methods

3.1. Sample preparation

Grains were extracted from crushed peridotite or megacryst fragments by handpicking under the optical microscope, mounted in epoxy and polished using standard procedures, including SiC and Al_2O_3 grinding and polishing grits. After polishing the mounts were washed in ethanol and carbon- or gold-coated for analysis.

3.2. Bulk analysis

Pure separates of the olivine grains were prepared by handpicking crushed, sieved and washed portions of the peridotite samples under the binocular microscope, excluding extraneous phases and altered grains, and keeping cracked grains to a minimum. Most separates were analyzed at the University of Maryland using techniques described by Aulbach et al. (2008). Li abundances and δ^{7}Li values for SC1-OL determined by MC-ICP-MS are from Seitz et al. (2004), and for the Ko'olau olivines by TIMS from Chan and Frey (2003).

3.3. SIMS analysis

Li isotope microanalyses were obtained on the Cameca IMS-3f and IMS-6f SIMS at Arizona State University. The primary beam was $^{16}O^{-}$ (15–30 nA, 30–50 μm diameter). Positive secondary ions with excess kinetic energies of 0±20 eV were detected in pulse counting mode. The mass spectrometer was operated at a mass resolving power that varied from ~600 to 1200 ($M/\Delta M$). Mass scans run at $M/\Delta M \sim 1200$ to separate ^{6}LiH from ^{7}Li consistently detected no hydride ion, even on hydrous glasses and clay minerals, so that most analyses were performed at lower mass resolution in order to maximize count rates and minimize counting statistics errors. Counting times were 10 s for ^{6}Li and 1 s for ^{7}Li in each cycle, with 50 to 200 cycles per analysis, and the largest contrast aperture (400 μm) was used. Typically a pre-sputter period of 3–5 min per point was employed. For the most recent analyses, including most analyses used in the matrix-effect calibration, charge compensation was evaluated every 20 cycles, and ranged from 0 to 30 V.

All raw $^{7}Li/^{6}Li$ isotope ratios and ^{7}Li intensity data were plotted as a function of cycle number to facilitate the screening of outliers and analyses affected by surface contamination or changes in primary ion intensity (as revealed by systematic trends or fluctuations in ^{7}Li count

Table 1
Olivine sample details

Sample no.	Fo±2σ	δ^{7}Li±2σ	Locality	Rock type	Reference
Mantle olivine samples used in matrix correction					
KBH-1	90.5±0.1	3.4±1.0	Kilbourne Hole, NM	Spinel lherzolite xenolith in basalt	1
SC1-OL	89.7	3.4±0.5	San Carlos, AZ	Spinel lherzolite xenolith in basalt	2
KPL-2	86.1±1.7	7.3±0.4	Hualalai, Hawai'i	Dunite xenolith in basalt	
LB51	85.5±1.7	6.6±0.3	Labait, Tanzania	Wehrlite xenolith in olivine melilitite	3, 5
LB29	92.4±0.3	3.5±0.7	Labait, Tanzania	Garnet lherzolite xenolith in olivine melilitite	3, 5
LB59	84.7±0.3	6.6±0.4	Labait, Tanzania	Wehrlite xenolith in olivine melilitite	3, 5
89-773	93.6±0.2	3.0±0.5	Olmani, Tanzania	Spinel harzburgite xenolith in ankaramite	4
PMD99-149	73.9±0.3	2.3±0.2	Gansfontein, South Africa	Olivine megacryst in kimberlite	6
MHK-1	52.4±0.3	−0.8±0.5	Mooihoek, South Africa	Dunite from pipe in Bushveld Complex	
Olivine phenocrysts from Hawaiian basalts					
KOO-17A	86.1–88.4	5.0±0.5	Makapu'u, O'ahu	Phenocrysts in lava flow	7
KOO-30A	81.8–88.3	2.6±0.5	Makapu'u, O'ahu	Phenocrysts in lava flow	7
KOO-49	78.1–85.5	2.3±0.7	Kamehame Ridge, O'ahu	Phenocrysts in lava flow	7
KOO-55	82.1–88.2	4.6±0.5	Kamehame Ridge, O'ahu	Phenocrysts in dike	7

Errors on olivine compositions represent compositional variability determined from numerous analyses (see text and Table A1). References refer to previous work on these olivines. Further references to the localities may be found in the text. 1. Bell and Rossman (1992), 2. Seitz et al. (2004), 3. Lee and Rudnick (1999), 4. Rudnick et al. (1994), 5. Aulbach et al. (2008), 6. Doyle (1999), 7. Chan and Frey (2003).

Table 2
Chemical compositions, bulk Li isotope compositions and SIMS (IMS-6f) Li isotope results for olivine samples used in matrix correction calibration

Sample	δ^7Li soln	^{7}Li/^{6}Li soln	FeO wt.%	Mg#	^{7}Li/^{6}Li$_{spl\ raw}$	δ^7Li$_{spl\ raw}$	^{7}Li/^{6}Li$_{std\ raw}$	β	^{7}Li/^{6}Li$_{spl\ cor}$	α cor	δ^7Li$_{spl\ rel\ KBH1}$	IMF (‰)
PMD99-149-1-1	2.3 (2)	12.200 (3)	23.9 (2)	73.9 (1)	12.647 (4)	38.9 (3)	12.400 (6)	1.0152	12.457 (10)	1.0211 (8)	23.7 (6)	21.4 (6)
PMD99-149-1-2	2.3 (2)	12.200 (3)	23.9 (2)	73.9 (1)	12.650 (4)	39.2 (3)	12.392 (16)	1.0145	12.469 (18)	1.0220 (15)	24.6 (13)	22.4 (14)
PMD99-149-2-1	2.3 (2)	12.200 (3)	23.9 (2)	73.9 (1)	12.653 (5)	39.4 (4)	12.400 (6)	1.0152	12.463 (10)	1.0215 (8)	24.2 (6)	21.9 (7)
PMD99-149-2-2	2.3 (2)	12.200 (3)	23.9 (2)	73.9 (1)	12.683 (4)	41.9 (4)	12.392 (16)	1.0145	12.502 (18)	1.0247 (15)	27.4 (13)	25.1 (14)
PMD99-149-3-1	2.3 (2)	12.200 (3)	23.9 (2)	73.9 (1)	12.649 (4)	39.1 (4)	12.400 (6)	1.0152	12.460 (10)	1.0213 (8)	23.9 (6)	21.6 (7)
PMD99-149-3-2	2.3 (2)	12.200 (3)	23.9 (2)	73.9 (1)	12.646 (4)	38.8 (4)	12.392 (16)	1.0145	12.464 (18)	1.0217 (15)	24.3 (13)	22.0 (14)
PMD99-149-4-1	2.3 (2)	12.200 (3)	23.9 (2)	73.9 (1)	12.643 (4)	38.6 (4)	12.400 (6)	1.0152	12.454 (10)	1.0208 (8)	23.4 (6)	21.1 (7)
PMD99-149-4-2	2.3 (2)	12.200 (3)	23.9 (2)	73.9 (1)	12.659 (5)	39.9 (4)	12.392 (16)	1.0145	12.478 (18)	1.0228 (15)	25.4 (13)	23.1 (14)
PMD99-149-5-1	2.3 (2)	12.200 (3)	23.9 (2)	73.9 (1)	12.650 (5)	39.2 (4)	12.400 (6)	1.0152	12.460 (10)	1.0213 (8)	23.9 (6)	21.7 (7)
PMD99-149-5-2	2.3 (2)	12.200 (3)	23.9 (2)	73.9 (1)	12.650 (4)	39.2 (3)	12.392 (16)	1.0145	12.469 (18)	1.0220 (15)	24.6 (13)	22.4 (13)
PMD99-149-6-1	2.3 (2)	12.200 (3)	23.9 (2)	73.9 (1)	12.644 (4)	38.7 (3)	12.400 (6)	1.0152	12.454 (10)	1.0208 (8)	23.4 (6)	21.2 (6)
PMD99-149-6-2	2.3 (2)	12.200 (3)	23.9 (2)	73.9 (1)	12.632 (4)	37.7 (3)	12.392 (16)	1.0145	12.451 (18)	1.0206 (15)	23.2 (13)	20.9 (13)
PMD99-149-6-3	2.3 (2)	12.200 (3)	23.9 (2)	73.9 (1)	12.647 (4)	39.0 (4)	12.400 (6)	1.0152	12.458 (10)	1.0211 (8)	23.7 (6)	21.4 (7)
PMD99-149 Avg	**2.3 (2)**	**12.200 (3)**	**23.9 (2)**	**73.9 (1)**	**12.647 (6)**	**39.0 (5)**			**12.461 (8)**	**1.0214 (7)**	**24.0 (6)**	**21.8 (7)**
89-773-1-1	3.0 (5)	12.210 (6)	6.37 (13)	93.6 (1)	12.409 (8)	19.4 (6)	12.400 (8)	1.0152	12.223 (12)	1.0011 (11)	4.1 (9)	1.1 (10)
89-773-1-2	3.0 (5)	12.210 (6)	6.37 (13)	93.6 (1)	12.400 (7)	18.6 (6)	12.408 (4)	1.0159	12.206 (10)	0.9997 (10)	2.7 (7)	−0.4 (8)
89-773-1-3	3.0 (5)	12.210 (6)	6.37 (13)	93.6 (1)	12.449 (9)	22.7 (7)	12.408 (4)	1.0159	12.254 (11)	1.0036 (10)	6.7 (8)	3.7 (9)
89-773-2-1	3.0 (5)	12.210 (6)	6.37 (13)	93.6 (1)	12.390 (8)	17.8 (7)	12.400 (8)	1.0152	12.204 (13)	0.9995 (11)	2.5 (9)	−0.5 (10)
89-773-3-1	3.0 (5)	12.210 (6)	6.37 (13)	93.6 (1)	12.346 (8)	14.2 (7)	12.400 (8)	1.0152	12.161 (13)	0.9960 (11)	−1.1 (9)	−4.1 (10)
89-773-3-2	3.0 (5)	12.210 (6)	6.37 (13)	93.6 (1)	12.350 (7)	14.6 (6)	12.408 (4)	1.0159	12.157 (10)	0.9957 (10)	−1.4 (7)	−4.4 (8)
89-773-4-1	3.0 (5)	12.210 (6)	6.37 (13)	93.6 (1)	12.368 (8)	16.0 (6)	12.400 (8)	1.0152	12.182 (12)	0.9977 (11)	0.7 (9)	−2.3 (10)
89-773-5-1	3.0 (5)	12.210 (6)	6.37 (13)	93.6 (1)	12.365 (7)	15.8 (6)	12.400 (8)	1.0152	12.179 (12)	0.9975 (11)	0.5 (9)	−2.6 (10)
89-773-6-1	3.0 (5)	12.210 (6)	6.37 (13)	93.6 (1)	12.386 (7)	17.5 (6)	12.400 (8)	1.0152	12.200 (12)	0.9992 (11)	2.2 (8)	−0.8 (10)
89-773-6-2	3.0 (5)	12.210 (6)	6.37 (13)	93.6 (1)	12.340 (8)	13.7 (7)	12.408 (4)	1.0159	12.147 (11)	0.9948 (10)	−2.2 (7)	−5.3 (9)
89-773-6-3	3.0 (5)	12.210 (6)	6.37 (13)	93.6 (1)	12.354 (9)	14.9 (7)	12.408 (4)	1.0159	12.161 (11)	0.9960 (10)	−1.1 (8)	−4.1 (9)
89-773-7-1	3.0 (5)	12.210 (6)	6.37 (13)	93.6 (1)	12.363 (8)	15.6 (7)	12.400 (8)	1.0152	12.177 (13)	0.9973 (11)	0.3 (9)	−2.7 (10)
89-773-7-2	3.0 (5)	12.210 (6)	6.37 (13)	93.6 (1)	12.371 (7)	16.3 (6)	12.400 (8)	1.0152	12.186 (12)	0.9980 (11)	1.0 (9)	−2.0 (10)
89-773-8-1	3.0 (5)	12.210 (6)	6.37 (13)	93.6 (1)	12.359 (7)	15.3 (6)	12.400 (8)	1.0152	12.174 (12)	0.9970 (11)	0.0 (9)	−3.0 (10)
89-773-8-2R	3.0 (5)	12.210 (6)	6.37 (13)	93.6 (1)	12.369 (8)	16.1 (6)	12.400 (8)	1.0152	12.183 (12)	0.9978 (11)	0.8 (9)	−2.2 (10)
89-773-9-1	3.0 (5)	12.210 (6)	6.37 (13)	93.6 (1)	12.364 (8)	15.7 (7)	12.400 (8)	1.0152	12.178 (13)	0.9974 (12)	0.4 (9)	−2.6 (11)
89-773-9-2R	3.0 (5)	12.210 (6)	6.37 (13)	93.6 (1)	12.354 (8)	14.9 (7)	12.400 (8)	1.0152	12.169 (13)	0.9966 (12)	−0.4 (9)	−3.4 (11)
89-773-10-1	3.0 (5)	12.210 (6)	6.37 (13)	93.6 (1)	12.357 (9)	15.1 (7)	12.400 (8)	1.0152	12.171 (13)	0.9969 (12)	−0.2 (9)	−3.2 (11)
89-773-10-2	3.0 (5)	12.210 (6)	6.37 (13)	93.6 (1)	12.356 (7)	15.0 (6)	12.400 (8)	1.0152	12.171 (12)	0.9968 (12)	−0.2 (9)	−3.3 (11)
89-773 Avg	**3.0 (5)**	**12.210 (6)**	**6.37 (13)**	**93.6 (1)**	**12.362 (13)**	**15.5 (11)**			**12.175 (15)**	**0.9971 (13)**	**0.1 (12)**	**−2.9 (13)**
KBH1_1	3.4 (5)	12.214 (6)	9.26 (10)	90.5 (1)	12.434 (6)	21.4 (5)	12.433 (7)	1.0179	12.215 (11)	1.0001 (10)	3.5 (7)	0.1 (9)
KBH1_2	3.4 (5)	12.214 (6)	9.26 (10)	90.5 (1)	12.437 (5)	21.7 (4)	12.433 (7)	1.0179	12.219 (11)	1.0004 (10)	3.8 (7)	0.4 (9)
KBH1_3	3.4 (5)	12.214 (6)	9.26 (10)	90.5 (1)	12.436 (5)	21.6 (4)	12.433 (7)	1.0179	12.217 (11)	1.0003 (10)	3.7 (7)	0.3 (9)
KBH1_4	3.4 (5)	12.214 (6)	9.26 (10)	90.5 (1)	12.418 (6)	20.1 (5)	12.433 (7)	1.0179	12.200 (11)	0.9988 (10)	2.2 (8)	−1.2 (9)
KBH1-1-1	3.4 (5)	12.214 (6)	9.26 (10)	90.5 (1)	12.426 (6)	20.8 (5)	12.421 (5)	1.0169	12.219 (10)	1.0004 (9)	3.8 (6)	0.4 (8)
KBH1-2-1	3.4 (5)	12.214 (6)	9.26 (10)	90.5 (1)	12.417 (6)	20.1 (5)	12.421 (5)	1.0169	12.211 (10)	0.9997 (9)	3.1 (6)	−0.3 (8)
KBH1-3-1	3.4 (5)	12.214 (6)	9.26 (10)	90.5 (1)	12.420 (6)	20.3 (5)	12.421 (5)	1.0169	12.213 (10)	0.9999 (9)	3.3 (6)	−0.1 (8)
KBH1-3-2	3.4 (5)	12.214 (6)	9.26 (10)	90.5 (1)	12.382 (7)	17.2 (6)	12.400 (8)	1.0152	12.196 (12)	0.9985 (11)	1.9 (8)	−1.5 (10)
KBH1-4-1	3.4 (5)	12.214 (6)	9.26 (10)	90.5 (1)	12.341 (8)	13.8 (6)	12.400 (8)	1.0152	12.156 (12)	0.9952 (11)	−1.5 (9)	−4.9 (10)
KBH1-2-2	3.4 (5)	12.214 (6)	9.26 (10)	90.5 (1)	12.405 (6)	19.0 (5)	12.400 (8)	1.0152	12.218 (12)	1.0003 (11)	3.7 (8)	0.3 (10)
KBH1-3-3	3.4 (5)	12.214 (6)	9.26 (10)	90.5 (1)	12.392 (6)	18.0 (5)	12.400 (8)	1.0152	12.206 (11)	0.9993 (11)	2.7 (8)	−0.7 (9)
KBH1-4-2	3.4 (5)	12.214 (6)	9.26 (10)	90.5 (1)	12.405 (7)	19.1 (6)	12.400 (8)	1.0152	12.219 (12)	1.0004 (11)	3.8 (8)	0.4 (10)
KBH1-2-3	3.4 (5)	12.214 (6)	9.26 (10)	90.5 (1)	12.433 (6)	21.4 (5)	12.400 (8)	1.0152	12.247 (12)	1.0026 (11)	6.1 (8)	2.7 (10)
KBH1-3-4	3.4 (5)	12.214 (6)	9.26 (10)	90.5 (1)	12.394 (6)	18.2 (5)	12.400 (8)	1.0152	12.209 (12)	0.9995 (11)	2.9 (8)	−0.5 (10)
KBH1-2-4	3.4 (5)	12.214 (6)	9.26 (10)	90.5 (1)	12.397 (7)	18.4 (6)	12.400 (8)	1.0152	12.211 (12)	0.9998 (11)	3.2 (8)	−0.2 (10)
KBH1-4-3	3.4 (5)	12.214 (6)	9.26 (10)	90.5 (1)	12.408 (5)	19.3 (5)	12.400 (8)	1.0152	12.223 (11)	1.0007 (10)	4.1 (8)	0.7 (9)
KBH1-3-5	3.4 (5)	12.214 (6)	9.26 (10)	90.5 (1)	12.409 (6)	19.4 (5)	12.408 (4)	1.0159	12.215 (9)	1.0000 (9)	3.4 (6)	0.0 (8)
KBH1-3-6	3.4 (5)	12.214 (6)	9.26 (10)	90.5 (1)	12.409 (6)	19.4 (5)	12.408 (4)	1.0159	12.215 (9)	1.0000 (9)	3.4 (6)	0.0 (8)
KBH1-2-5	3.4 (5)	12.214 (6)	9.26 (10)	90.5 (1)	12.408 (6)	19.3 (5)	12.408 (4)	1.0159	12.214 (9)	0.9999 (9)	3.3 (6)	−0.1 (8)
KBH1-3-7	3.4 (5)	12.214 (6)	9.26 (10)	90.5 (1)	12.394 (6)	18.2 (5)	12.400 (6)	1.0152	12.209 (11)	0.9995 (10)	2.9 (7)	−0.5 (9)
KBH1-3-8	3.4 (5)	12.214 (6)	9.26 (10)	90.5 (1)	12.410 (6)	19.5 (5)	12.400 (6)	1.0152	12.224 (10)	1.0008 (10)	4.2 (7)	0.8 (9)
KBH1-4-4	3.4 (5)	12.214 (6)	9.26 (10)	90.5 (1)	12.396 (6)	18.3 (5)	12.400 (6)	1.0152	12.210 (10)	0.9996 (10)	3.0 (7)	−0.4 (9)
KBH1-2-7	3.4 (5)	12.214 (6)	9.26 (10)	90.5 (1)	12.399 (5)	18.6 (4)	12.400 (6)	1.0152	12.213 (10)	0.9999 (10)	3.3 (7)	−0.1 (8)
KBH1-2-8	3.4 (5)	12.214 (6)	9.26 (10)	90.5 (1)	12.402 (7)	18.8 (5)	12.400 (6)	1.0152	12.216 (11)	1.0001 (10)	3.5 (7)	0.1 (9)
KBH1-3-9	3.4 (5)	12.214 (6)	9.26 (10)	90.5 (1)	12.377 (6)	16.8 (5)	12.392 (16)	1.0145	12.200 (18)	0.9988 (15)	2.2 (14)	−1.2 (15)
KBH1-3-10	3.4 (5)	12.214 (6)	9.26 (10)	90.5 (1)	12.408 (5)	19.4 (4)	12.392 (16)	1.0145	12.231 (18)	1.0014 (15)	4.8 (14)	1.4 (15)
KBH1-2-9	3.4 (5)	12.214 (6)	9.26 (10)	90.5 (1)	12.389 (6)	17.8 (5)	12.392 (16)	1.0145	12.212 (18)	0.9998 (16)	3.2 (14)	−0.2 (15)
KBH1-2-10	3.4 (5)	12.214 (6)	9.26 (10)	90.5 (1)	12.391 (6)	17.9 (5)	12.392 (16)	1.0145	12.213 (18)	0.9999 (15)	3.3 (14)	−0.1 (15)
KBH1-3-11	3.4 (5)	12.214 (6)	9.26 (10)	90.5 (1)	12.375 (5)	16.6 (4)	12.386 (9)	1.0141	12.203 (12)	0.9991 (11)	2.5 (8)	−0.9 (10)
KBH1-3-12	3.4 (5)	12.214 (6)	9.26 (10)	90.5 (1)	12.384 (6)	17.3 (5)	12.386 (9)	1.0141	12.212 (12)	0.9998 (11)	3.2 (8)	−0.2 (10)
KBH1-3	3.4 (5)	12.214 (6)	9.26 (10)	90.5 (1)	12.393 (6)	18.1 (5)	12.386 (9)	1.0141	12.221 (12)	1.0006 (11)	4.0 (9)	0.6 (10)
KBH1-3-14	3.4 (5)	12.214 (6)	9.26 (10)	90.5 (1)	12.394 (6)	18.2 (5)	12.386 (9)	1.0141	12.222 (12)	1.0007 (11)	4.1 (8)	0.7 (10)
KBH1-2-11	3.4 (5)	12.214 (6)	9.26 (10)	90.5 (1)	12.397 (6)	18.4 (5)	12.386 (9)	1.0141	12.225 (12)	1.0009 (11)	4.3 (9)	0.9 (10)
KBH1-4-6	3.4 (5)	12.214 (6)	9.26 (10)	90.5 (1)	12.385 (7)	17.4 (5)	12.386 (9)	1.0141	12.213 (12)	0.9999 (11)	3.3 (9)	−0.1 (10)
KBH1-4-7	3.4 (5)	12.214 (6)	9.26 (10)	90.5 (1)	12.375 (5)	16.6 (4)	12.386 (9)	1.0141	12.204 (12)	0.9991 (11)	2.5 (8)	−0.9 (10)
KBH1-3-15	3.4 (5)	12.214 (6)	9.26 (10)	90.5 (1)	12.385 (6)	17.5 (5)	12.386 (9)	1.0141	12.214 (12)	0.9999 (11)	3.3 (8)	−0.1 (10)
KBH-1 Avg	**3.4 (5)**	**12.214 (6)**	**9.26 (10)**	**90.5 (1)**	**12.402 (17)**	**18.8 (14)**			**12.214 (7)**	**1.0000 (8)**	**3.4 (6)**	**0.0 (8)**
KPL2-3-1	7.3 (4)	12.261 (5)	13.13 (10)	86.3 (1)	12.500 (6)	26.8 (5)	12.421 (5)	1.0169	12.292 (10)	1.0025 (9)	9.9 (6)	2.6 (7)

(continued on next page)

Table 2 (*continued*)

Sample	δ^7Li soln	^{7}Li/^{6}Li soln	FeO wt.%	Mg#	^{7}Li/^{6}Li$_{spl\ raw}$	δ^7Li$_{spl\ raw}$	^{7}Li/^{6}Li$_{std\ raw}$	β	^{7}Li/^{6}Li$_{spl\ cor}$	α cor	δ^7Li$_{spl\ rel\ KBH1}$	IMF (‰)
KPL2-4-1	7.3 (4)	12.261 (5)	12.75 (10)	86.9 (1)	12.509 (5)	27.6 (4)	12.421 (5)	1.0169	12.301 (9)	1.0032 (8)	10.6 (5)	3.4 (7)
KPL2-4-2R	7.3 (4)	12.261 (5)	12.62 (10)	86.9 (1)	12.485 (5)	25.6 (4)	12.421 (5)	1.0169	12.277 (9)	1.0013 (8)	8.6 (6)	1.4 (7)
KPL2-6-1	7.3 (4)	12.261 (5)	12.67 (20)	86.9 (2)	12.487 (6)	25.8 (5)	12.400 (3)	1.0152	12.299 (8)	1.0031 (8)	10.5 (5)	3.2 (6)
KPL2-a Avg	**7.3 (4)**	**12.261 (5)**	**12.79 (23)**	**86.8 (3)**	**12.495 (11)**	**26.5 (9)**			**12.292 (11)**	**1.0025 (10)**	**9.9 (9)**	**2.6 (10)**
KPL2-7-1	7.3 (4)	12.261 (5)	14.38 (10)	84.9 (1)	12.536 (6)	29.8 (5)	12.400 (3)	1.0152	12.348 (8)	1.0071 (8)	14.5 (5)	7.3 (6)
KPL2-7-2	7.3 (4)	12.261 (5)	14.36 (10)	84.8 (1)	12.525 (5)	28.9 (4)	12.400 (3)	1.0152	12.337 (8)	1.0062 (7)	13.6 (4)	6.4 (5)
KPL2-7-3	7.3 (4)	12.261 (5)	14.39 (10)	84.8 (1)	12.544 (5)	30.5 (4)	12.400 (3)	1.0152	12.356 (8)	1.0077 (7)	15.2 (4)	8.0 (5)
KPL2-b Avg	**7.3 (4)**	**12.261 (5)**	**14.38 (6)**	**84.9 (1)**	**12.535 (10)**	**29.8 (8)**			**12.347 (10)**	**1.0070 (9)**	**14.5 (8)**	**7.2 (9)**
LB29-3-1	3.5 (7)	12.215 (9)	7.50 (17)	92.4 (1)	12.370 (6)	16.2 (5)	12.400 (8)	1.0152	12.185 (11)	0.9976 (12)	1.0 (8)	−2.5 (11)
LB29-3-2	3.5 (7)	12.215 (9)	7.50 (17)	92.4 (1)	12.381 (7)	17.1 (5)	12.400 (8)	1.0152	12.196 (12)	0.9985 (12)	1.9 (8)	−1.6 (11)
LB29-3-3	3.5 (7)	12.215 (9)	7.50 (17)	92.4 (1)	12.376 (6)	16.7 (5)	12.400 (8)	1.0152	12.191 (11)	0.9980 (12)	1.4 (8)	−2.0 (11)
LB29-3-4	3.5 (7)	12.215 (9)	7.50 (17)	92.4 (1)	12.384 (6)	17.3 (5)	12.400 (8)	1.0152	12.199 (11)	0.9987 (12)	2.1 (8)	−1.4 (11)
LB29-3-5	3.5 (7)	12.215 (9)	7.50 (17)	92.4 (1)	12.393 (7)	18.1 (6)	12.400 (8)	1.0152	12.208 (12)	0.9994 (12)	2.9 (8)	−0.6 (11)
LB29-3-6	3.5 (7)	12.215 (9)	7.50 (17)	92.4 (1)	12.391 (6)	17.9 (5)	12.400 (8)	1.0152	12.206 (11)	0.9993 (12)	2.7 (8)	−0.7 (11)
LB29-4-1	3.5 (7)	12.215 (9)	7.50 (17)	92.4 (1)	12.374 (6)	16.5 (5)	12.400 (8)	1.0152	12.189 (11)	0.9978 (12)	1.3 (8)	−2.2 (11)
LB29-4-2	3.5 (7)	12.215 (9)	7.50 (17)	92.4 (1)	12.375 (6)	16.6 (5)	12.400 (8)	1.0152	12.190 (12)	0.9980 (12)	1.4 (8)	−2.1 (11)
LB29-5-1	3.5 (7)	12.215 (9)	7.50 (17)	92.4 (1)	12.389 (7)	17.7 (5)	12.400 (8)	1.0152	12.203 (12)	0.9991 (12)	2.5 (8)	−1.0 (11)
LB29-6-1	3.5 (7)	12.215 (9)	7.50 (17)	92.4 (1)	12.384 (5)	17.4 (4)	12.400 (8)	1.0152	12.199 (11)	0.9987 (11)	2.1 (7)	−1.3 (10)
LB29 Avg	**3.5 (7)**	**12.215 (9)**	**7.50 (17)**	**92.4 (2)**	**12.382 (8)**	**17.2 (6)**			**12.197 (8)**	**0.9985 (10)**	**1.9 (6)**	**−1.5 (10)**
LB51-1-1	6.6 (3)	12.253 (4)	13.99 (27)	85.5 (2)	12.578 (5)	33.3 (4)	12.421 (5)	1.0169	12.369 (9)	1.0095 (8)	16.3 (5)	9.8 (6)
LB51-2-1	6.6 (3)	12.253 (4)	14.01 (20)	85.3 (2)	12.578 (4)	33.3 (4)	12.421 (5)	1.0169	12.369 (9)	1.0095 (8)	16.3 (5)	9.7 (6)
LB51-3-1	6.6 (3)	12.253 (4)	14.01 (20)	85.3 (2)	12.617 (5)	36.5 (4)	12.421 (5)	1.0169	12.407 (9)	1.0126 (8)	19.5 (6)	12.9 (6)
LB51-3-2	6.6 (3)	12.253 (4)	14.11 (20)	85.2 (2)	12.610 (5)	35.9 (4)	12.421 (5)	1.0169	12.400 (9)	1.0120 (8)	18.9 (5)	12.4 (6)
LB51-3-3	6.6 (3)	12.253 (4)	13.91 (20)	85.4 (2)	12.603 (5)	35.3 (4)	12.421 (5)	1.0169	12.393 (9)	1.0115 (8)	18.4 (6)	11.8 (6)
LB51-3-4	6.6 (3)	12.253 (4)	14.19 (20)	85.2 (2)	12.594 (5)	34.6 (4)	12.421 (5)	1.0169	12.385 (9)	1.0108 (8)	17.7 (5)	11.1 (6)
LB51-3-5	6.6 (3)	12.253 (4)	14.31 (20)	85.1 (2)	12.592 (5)	34.5 (4)	12.421 (5)	1.0169	12.383 (9)	1.0106 (8)	17.5 (5)	11.0 (6)
LB51-3-6	6.6 (3)	12.253 (4)	14.58 (20)	84.9 (2)	12.582 (6)	33.6 (5)	12.421 (5)	1.0169	12.373 (10)	1.0098 (8)	16.6 (6)	10.1 (7)
LB51-3-7	6.6 (3)	12.253 (4)	14.67 (20)	84.7 (2)	12.569 (5)	32.5 (4)	12.421 (5)	1.0169	12.360 (9)	1.0088 (8)	15.6 (6)	9.0 (6)
LB51-3-8	6.6 (3)	12.253 (4)	14.67 (20)	84.7 (2)	12.583 (4)	33.7 (4)	12.421 (5)	1.0169	12.374 (9)	1.0099 (8)	16.8 (5)	10.2 (6)
LB51-4-1	6.6 (3)	12.253 (4)	12.24 (20)	87.2 (2)	12.510 (5)	27.7 (4)	12.392 (16)	1.0145	12.331 (18)	1.0064 (15)	13.1 (13)	6.6 (14)
LB51-4-2	6.6 (3)	12.253 (4)	12.53 (20)	86.9 (2)	12.514 (4)	28.0 (4)	12.392 (16)	1.0145	12.335 (18)	1.0067 (15)	13.5 (13)	6.9 (14)
LB51-4-3	6.6 (3)	12.253 (4)	12.28 (20)	87.2 (2)	12.513 (6)	28.0 (5)	12.392 (16)	1.0145	12.334 (18)	1.0067 (15)	13.4 (14)	6.8 (14)
LB51-4-4	6.6 (3)	12.253 (4)	12.56 (20)	87.0 (2)	12.533 (4)	29.6 (4)	12.392 (16)	1.0145	12.353 (18)	1.0082 (15)	15.0 (13)	8.4 (14)
LB51-5-1	6.6 (3)	12.253 (4)	14.45 (20)	84.7 (2)	12.537 (4)	29.9 (4)	12.400 (3)	1.0152	12.349 (7)	1.0078 (7)	14.6 (4)	8.1 (5)
LB51-5-2	6.6 (3)	12.253 (4)	14.34 (20)	84.9 (2)	12.537 (4)	29.9 (3)	12.400 (3)	1.0152	12.349 (7)	1.0078 (7)	14.6 (3)	8.1 (4)
LB51-5-3	6.6 (3)	12.253 (4)	14.68 (20)	84.6 (2)	12.547 (5)	30.7 (4)	12.400 (3)	1.0152	12.358 (8)	1.0086 (7)	15.4 (4)	8.9 (5)
LB51-6-1	6.6 (3)	12.253 (4)	14.39 (20)	85.1 (2)	12.548 (5)	30.8 (4)	12.400 (3)	1.0152	12.359 (8)	1.0087 (7)	15.5 (4)	8.9 (5)
LB51-6-2	6.6 (3)	12.253 (4)	14.12 (20)	85.3 (2)	12.539 (4)	30.1 (4)	12.400 (3)	1.0152	12.351 (8)	1.0080 (7)	14.8 (4)	8.3 (5)
LB51-6-3	6.6 (3)	12.253 (4)	13.96 (20)	85.5 (2)	12.541 (4)	30.3 (4)	12.400 (3)	1.0152	12.353 (7)	1.0082 (7)	15.0 (4)	8.4 (5)
LB51 Avg	**6.6 (3)**	**12.253 (4)**	**13.90 (81)**	**85.5 (9)**	**12.561 (33)**	**31.9 (27)**			**12.364 (22)**	**1.0091 (18)**	**15.9 (18)**	**9.4 (18)**
LB59-1-1	6.6 (4)	12.253 (5)	14.61 (19)	84.7 (2)	12.580 (5)	33.4 (4)	12.408 (4)	1.0159	12.383 (9)	1.0106 (8)	17.5 (5)	10.9 (6)
LB59-1-2	6.6 (4)	12.253 (5)	14.61 (19)	84.7 (2)	12.581 (5)	33.5 (4)	12.408 (4)	1.0159	12.384 (9)	1.0107 (8)	17.6 (5)	11.0 (6)
LB59-2-1	6.6 (4)	12.253 (5)	14.61 (19)	84.7 (2)	12.582 (5)	33.6 (4)	12.408 (4)	1.0159	12.385 (9)	1.0108 (8)	17.7 (5)	11.1 (6)
LB59-3-1	6.6 (4)	12.253 (5)	14.61 (19)	84.7 (2)	12.579 (4)	33.4 (3)	12.408 (4)	1.0159	12.382 (8)	1.0105 (8)	17.4 (4)	10.8 (6)
LB59-4-1	6.6 (4)	12.253 (5)	14.61 (19)	84.7 (2)	12.576 (5)	33.1 (4)	12.408 (4)	1.0159	12.379 (8)	1.0103 (8)	17.2 (5)	10.6 (6)
LB59-5-1	6.6 (4)	12.253 (5)	14.61 (19)	84.7 (2)	12.567 (4)	32.3 (4)	12.408 (4)	1.0159	12.370 (8)	1.0095 (8)	16.4 (5)	9.8 (6)
LB59-6-1	6.6 (4)	12.253 (5)	14.61 (19)	84.7 (2)	12.582 (4)	33.6 (4)	12.408 (4)	1.0159	12.385 (8)	1.0107 (8)	17.6 (5)	11.0 (6)
LB59-7-1	6.6 (4)	12.253 (5)	14.61 (19)	84.7 (2)	12.580 (5)	33.5 (4)	12.408 (4)	1.0159	12.383 (9)	1.0106 (8)	17.5 (5)	10.9 (6)
LB59-8-1	6.6 (4)	12.253 (5)	14.61 (19)	84.7 (2)	12.569 (5)	32.5 (4)	12.408 (4)	1.0159	12.372 (9)	1.0097 (8)	16.6 (5)	9.9 (6)
LB59 Avg	**6.6 (4)**	**12.253 (5)**	**14.61 (19)**	**84.7 (2)**	**12.577 (6)**	**33.2 (5)**			**12.380 (6)**	**1.0104 (6)**	**17.3 (5)**	**10.7 (6)**
SC1 Ol-1-1	3.4 (5)	12.214 (6)	10.10 (10)	89.6 (1)	12.432 (5)	21.3 (4)	12.435 (7)	1.0181	12.211 (11)	0.9998 (10)	3.1 (7)	−0.3 (9)
SC1 Ol-1-2	3.4 (5)	12.214 (6)	10.10 (10)	89.6 (1)	12.443 (4)	22.2 (4)	12.435 (7)	1.0181	12.222 (10)	1.0007 (10)	4.1 (7)	0.7 (8)
SC1 Ol-1-3	3.4 (5)	12.214 (6)	10.10 (10)	89.6 (1)	12.428 (5)	21.0 (4)	12.435 (7)	1.0181	12.208 (10)	0.9995 (10)	2.9 (7)	−0.5 (9)
SC1-OL1 Avg	**3.4 (5)**	**12.214 (6)**	**10.10 (10)**	**89.6 (1)**	**12.434 (8)**	**21.5 (6)**			**12.214 (8)**	**1.0000 (8)**	**3.4 (6)**	**0.0 (8)**
MHK-1-0	−0.8 (5)	12.163 (6)	39.7 (4)	52.4 (3)	11.955 (8)	−17.9 (7)	11.907 (9)	0.9749	12.263 (14)	1.0082 (13)	7.3 (10)	8.1 (12)
MHK-1-1	−0.8 (5)	12.163 (6)	39.7 (4)	52.4 (3)	11.943 (7)	−18.9 (6)	11.907 (9)	0.9749	12.251 (14)	1.0072 (12)	6.3 (10)	7.1 (11)
MHK-1-2	−0.8 (5)	12.163 (6)	39.7 (4)	52.4 (3)	11.949 (7)	−18.4 (6)	11.907 (9)	0.9749	12.257 (14)	1.0078 (12)	6.9 (10)	7.7 (11)
MHK-1-3	−0.8 (5)	12.163 (6)	39.7 (4)	52.4 (3)	11.963 (10)	−17.2 (8)	11.907 (9)	0.9749	12.272 (15)	1.0089 (14)	8.0 (12)	8.8 (13)
MHK-1-4	−0.8 (5)	12.163 (6)	39.7 (4)	52.4 (3)	11.978 (8)	−16.0 (7)	11.907 (9)	0.9749	12.287 (14)	1.0102 (13)	9.2 (10)	10.0 (11)
MHK-1-5	−0.8 (5)	12.163 (6)	39.7 (4)	52.4 (3)	11.979 (9)	−15.9 (7)	11.907 (9)	0.9749	12.288 (15)	1.0103 (13)	9.3 (11)	10.1 (12)
MHK-1-6	−0.8 (5)	12.163 (6)	39.7 (4)	52.4 (3)	11.984 (8)	−15.5 (7)	11.907 (9)	0.9749	12.293 (14)	1.0107 (13)	9.7 (10)	10.5 (12)
MHK-1-7	−0.8 (5)	12.163 (6)	39.7 (4)	52.4 (3)	11.976 (7)	−16.1 (6)	11.907 (9)	0.9749	12.285 (14)	1.0100 (12)	9.1 (10)	9.9 (11)
MHK-1-8	−0.8 (5)	12.163 (6)	39.7 (4)	52.4 (3)	11.986 (7)	−15.4 (5)	11.907 (9)	0.9749	12.295 (13)	1.0108 (12)	9.9 (10)	10.7 (11)
MHK-1-9	−0.8 (5)	12.163 (6)	39.7 (4)	52.4 (3)	11.977 (6)	−16.1 (5)	11.907 (9)	0.9749	12.286 (13)	1.0101 (12)	9.1 (9)	9.9 (11)
MHK-1-10	−0.8 (5)	12.163 (6)	39.7 (4)	52.4 (3)	11.973 (7)	−16.4 (6)	11.907 (9)	0.9749	12.282 (13)	1.0098 (12)	8.8 (10)	9.6 (11)
MHK-1-11	−0.8 (5)	12.163 (6)	39.7 (4)	52.4 (3)	11.962 (8)	−17.3 (7)	11.907 (9)	0.9749	12.270 (14)	1.0088 (13)	7.9 (10)	8.7 (12)
MHK-1-12	−0.8 (5)	12.163 (6)	39.7 (4)	52.4 (3)	11.975 (8)	−16.2 (7)	11.907 (9)	0.9749	12.284 (14)	1.0100 (13)	9.0 (10)	9.8 (12)
MHK-1-13	−0.8 (5)	12.163 (6)	39.7 (4)	52.4 (3)	11.988 (8)	−15.2 (7)	11.907 (9)	0.9749	12.297 (14)	1.0110 (13)	10.0 (11)	10.8 (12)
MHK-1-14	−0.8 (5)	12.163 (6)	39.7 (4)	52.4 (3)	11.990 (8)	−15.0 (7)	11.907 (9)	0.9749	12.300 (14)	1.0112 (13)	10.2 (11)	11.0 (12)
MHK-1-15	−0.8 (5)	12.163 (6)	39.7 (4)	52.4 (3)	11.974 (9)	−16.4 (8)	11.907 (9)	0.9749	12.283 (15)	1.0098 (13)	8.9 (11)	9.7 (12)
MHK-1 Avg	**-0.8 (5)**	**12.163 (6)**	**39.7 (4)**	**52.4 (3)**	**11.972 (14)**	**−16.5 (11)**			**12.281 (14)**	**1.0097 (13)**	**8.7 (11)**	**9.5 (12)**

rate). This monitoring of each analysis also reveals if systematic changes in $^{7}Li/^{6}Li$ arise as a function of crater geometry as sputtering progresses. We observed no such systematic variation for olivine under the conditions employed in this study; such effects in the analysis of basaltic glasses have been noticed intermittently by us and others (University of Edinburgh SIMS lab, personal communication to RLH) with no clear cause of this effect. Because of the apparent insensitivity of the $^{7}Li/^{6}Li$ in olivine to time of sputtering up to 200 cycles, variations in primary beam current which affect sputtering rate also have no observable effect on the $^{7}Li/^{6}Li$ ratio within the limits applied here. Traces of Li derived from vacuum grease used in preparation of isolated examples of epoxy mounts sometimes affected the near-surface isotope composition of grains, especially close to grain edges where grease could be spread from the interface between the grain and the enclosing epoxy. Although the isotopic effects of minor grease contamination are potentially severe, they were effectively removed by the screening procedure. The isotopic composition of ~+250‰ (deduced from a comparative study of contaminated and uncontaminated grains) is consistent with certain batches of laboratory lithium residual from an isotope enrichment program surrounding fusion research (Qi et al., 1997).

The $^{7}Li/^{6}Li$ ratios determined by SIMS were referenced to an olivine standard in order to eliminate as far as possible the effect of variations in instrumental settings and analytical conditions. In most runs this was an olivine from the Kilbourne Hole spinel lherzolite KBH-1 (Bell and Rossman, 1992), usually mounted with the sample. This is an in-house secondary standard that we determined to be indistinguishable in its Li isotope composition from SC-1 Ol, a spinel lherzolite olivine from San Carlos provided by H.-M. Seitz. The SC-1 Ol standard has a $\delta^{7}Li$ of 3.4±0.5‰ (2σ, $n=5$) determined by MC-ICP-MS (Seitz et al., 2004). No significant isotopic zoning such as that observed by Jeffcoate et al. (2007) in a xenolith from San Carlos was seen in the olivine from SC1 analyzed in this study. Li isotope compositions are expressed as $\delta^{7}Li$ relative to the L-SVEC standard ($^{7}Li/^{6}Li=12.1729$; Qi et al., 1997), so that the true $^{7}Li/^{6}Li$ for KBH-1 is assumed to be 12.2143. Typically, analyses of KBH-1 were performed at intervals throughout the analytical sessions. Usually, these were the average of 3 or 4 analyses on different grains. Where standard drift was observed, the standard value appropriate to each analysis was assigned by interpolation. This procedure contributes some uncertainty to the analysis because it is not always possible to tell whether the variation is due to instrument drift or some minor heterogeneity in the standard. During the analysis of numerous grains of KBH1 over the past four years we have occasionally observed heterogeneity in $\delta^{7}Li$ at the edge of some grains, or in one or two exceptional grains. Efforts were made to avoid such regions. However, it is possible that some minor heterogeneity in the standard contributes to the overall uncertainty in our treatment.

Accumulated uncertainties in determination of the matrix correction (including inter- and intra-granular compositional and isotopic variability of olivine in mineral separates) imply that the matrix correction introduces additional uncertainty to the reported isotopic compositions. The uncertainty in this correction is minimized by using a standard near the middle of the compositional range of our sample suite (Fo74–95). In the case of KBH1 (Fo90.5) the maximum added uncertainty at the compositional extremes is 0.5‰. The disadvantage of the KBH-1 standard is that its Li content is relatively low (1.2 ppm) so that the standard error of a single analysis for typical primary beam currents of 15–30 nA is in the range of 0.7–1‰ ($1\sigma_{mean}$, 100 cycles). Consequently, groups of 3–5 analyses of the standard were performed at regular intervals throughout an analytical session, and the standard $^{7}Li/^{6}Li$ inferred by interpolation.

Analytical errors for each point (the standard error of the mean of the total number of isotope ratio measurements—typically 100) were within 0 to 0.3‰ of the theoretical error expected from counting statistics alone (i.e., the error based on Poisson statistics of total counts). Relative uncertainties decreased with increasing Li concentration in the analyzed phase, determined qualitatively from the ^{7}Li count rate. Count rates among phases studied varied by a factor of six, reflecting the variation in Li concentration, with lower count rates requiring more cycles to achieve the desired standard error of ±1‰ (1σ) or better.

For most peridotites used in the calibration, from five to nine grains were mounted and from one to three $^{7}Li/^{6}Li$ analyses performed per grain. However, for some of the low-Li samples (low-temperature peridotites), multiple step scans across grains were performed in automated mode. For the most part such scans showed homogeneous $\delta^{7}Li$ within $\pm1\sigma$, but in some grains an increase in $\delta^{7}Li$ at the grain margin was observed, and occasional internal points showed anomalous excursions to low $\delta^{7}Li$. These outliers were not considered in computation of the mean $\delta^{7}Li$ values reported in Table 2. Where the variability exceeds $\pm2\sigma$ counting statistics errors of individual analyses, and cannot be ascribed to clear outliers, we conclude that the sample is heterogeneous and the errors are quoted as standard deviations (σ), rather than standard errors ($\sigma/\sqrt{n}$). The origins of the intra-grain $\delta^{7}Li$ heterogeneities in xenoliths are under further investigation.

Li concentration estimates by TIMS or MC-ICP-MS are available for some of the bulk separates of olivine (Chan and Frey, 2003; Seitz et al., 2004; Aulbach et al., 2008). For the Ko'olau olivines, we determined relative variations in Li concentration within grains or among grains of the same sample from the raw ^{7}Li count rates determined relative to a standard over a limited operating time on the SIMS. We used KBH-1 which has 1.19±0.08 (2σ) ppm Li, determined by SIMS analysis calibrated against SC1-OL (1.70±0.07 (2σ) ppm Li—Seitz et al., 2004). These two olivines have extremely similar compositions, so any matrix effects of SIMS analysis will be negligible. Typical olivine analyses on the ASU SIMS show an increasing ^{7}Li count rate, leveling off as analysis proceeds. For this reason, the average of the ^{7}Li counts over the last 50 cycles was averaged, rather than using all 100 cycles.

The accuracy of Li abundances determined by this method was evaluated with reference to a number of standard glasses, and also with reference to more traditional analysis using both energy-filtered $^{7}Li^{+}/^{30}Si^{+}$ ratios collected at −75 V offset and $^{7}Li^{+}/^{28}Si^{+}$ ratios collected at 0 V offset (Fig. A1, supporting online material). Agreement between the KBH-1 standardization tied to SC1-OL and that for basaltic glasses (Kasemann et al., 2005) under the same measurement conditions is excellent. Agreement with high-silica glasses UTR-2 and NIST-610 is less impressive, but within 20%. Li abundances in olivine determined

Notes to Table 2:
$\delta^{7}Li$ soln and $^{7}Li/^{6}Li$ soln: Values determined by MC-ICP-MS at the Univ. Maryland with the exception of SC1-OL (Seitz et al., 2004).
Wt.% FeO and Mg# [=100 Mg/(Mg+Fe)] determined by electron microprobe at ASU.
$^{7}Li/^{6}Li_{spl\ raw}$ and $^{7}Li/^{6}Li_{std\ raw}$: Uncorrected raw Li isotope compositions by SIMS (IMS-6f) for sample and standard respectively.
$\delta^{7}Li_{spl\ raw}=1000*[(^{7}Li/^{6}Li_{spl,\ raw}/12.1729)-1]$.
$\beta=[^{7}Li/^{6}Li_{std,\ raw}]/[^{7}Li/^{6}Li_{std,\ true}]=[^{7}Li/^{6}Li_{std,\ raw}]/12.2143$.
$^{7}Li/^{6}Li\ cor=[^{7}Li/^{6}Li_{raw}]/\beta$.
$\alpha_{cor}=[^{7}Li/^{6}Li_{cor}]/[^{7}Li/^{6}Li_{soln}]$.
$\delta^{7}Li_{rel\ KBH1}=1000*([^{7}Li/^{6}Li_{spl,raw}]/[^{7}Li/^{6}Li_{KBH1,raw}]-1)+3.40$.
$IMF=\delta^{7}Li_{rel\ KBH1}-\delta^{7}Li_{soln}$.
Parentheses indicate 1σ uncertainties in the last digit. Uncertainties in individual raw SIMS data are standard errors of the mean of 100 analyses, with uncertainties for derivative parameters propagated as described by Bevington and Robinson (2002). Uncertainty in solution data are standard deviations of repeat analyses.
Uncertainties for sample averages (bold) are standard deviations of the mean of the individual analyses listed. All errors are 1s. $\delta^{7}Li$ values for samples of BHVO-2G and BCR-2G basalt glasses determined using the KBH1 standard are 20.0±1.7 and 16.5±1.7‰, respectively.

using both the $^{7}Li^{+}$ intensities and $^{7}Li^{+}/^{28}Si^{+}$ at 0 V offset agree well with those determined using the $^{7}Li^{+}/^{30}Si^{+}$ ratios collected at −75 V for samples with low Li contents, but begin to diverge to lower values at Li>~2.5 ppm, and are up to 50% lower at 10 ppm. High-Li olivines are also high in Fe, suggesting to us that the physical cause of this divergence is related to the fayalite content of the olivine, rather than the Li content. The divergence occurs at Fe contents similar to those where the greatest variations in isotopic matrix effects occur. This evidence for a matrix effect on Li abundance measurements requires further investigation. However, its influence on the Li abundance data discussed in this paper for the Ko'olau olivines (which all have Fo>78) is negligible, the maximum effect being ~10% relative.

3.4. Electron microprobe analysis

Compositions of the samples used for matrix-effect calibration and of the Ko'olau phenocryst olivines were determined on the JEOL8600 microprobe at ASU. Analyses were conducted with a focused 30–40 nA electron beam, with 10–30 s peak-counting times. A natural olivine standard was used for all major elements. Raw data were reduced with the CITZAF procedure (Armstrong, 1988).

Detailed electron microprobe analysis of all olivine grains was conducted after SIMS analysis of Li isotopes. Several analyses were performed adjacent to SIMS craters, and typically the crater compositions were estimated by averaging surrounding electron probe data. Uncertainties in composition for each spot reported in Table 3 reflect the standard deviation of the surrounding analyses. Compositions were also determined in other areas of grains to examine the extent of zoning and any relationship to grain morphology. In cases where grains were found to be homogeneous within the uncertainties of microprobe analysis, the same mean composition was assigned to each SIMS point analyzed. Unfortunately, compositional variations are not easily related to original grain boundaries because many grains break during the mineral separation processing. 245 electron microprobe analyses were used to define the compositions of the SIMS analyses of the phenocryst and mantle samples used to evaluate matrix effects.

4. Results of the matrix effect calibration

Li isotope data for the peridotite samples used in the matrix effect correction are listed in Table 2. Individual spot analyses as well as sample averages are reported. An extended version of Table 2 is given as Table A1 in the electronic appendix. The full dataset of individual δ^{7}Li analyses (including the Hawaiian olivines) *uncorrected* for any composition-dependent instrumental mass fractionation (IMF) and plotted as a function of Mg# (Fig. 1) shows the clear tendency for δ^{7}Li to increase with decreasing Fo content of the olivine. The compositional dependence of IMF (matrix effect) is illustrated by plotting for each sample the difference between the average δ^{7}Li determined by SIMS and the bulk solution δ^{7}Li by MC-ICP-MS or TIMS (Fig. 2). A linear regression of these data shows that the matrix effect is 1.3‰ per Fo unit, demonstrating that olivine composition must be precisely known for accurate Li isotope analysis by SIMS.

4.1. Linear calibration for Fe-poor olivines

If $[^{7}Li/^{6}Li_{std,\,raw}]$ and $[^{7}Li/^{6}Li_{spl,\,raw}]$ are the raw SIMS $^{7}Li/^{6}Li$ isotope ratios on the standard and sample, respectively, then these are related to the true $^{7}Li/^{6}Li$ isotope ratios in the standard and sample by the instrumental mass fractionation factors α and β:

$$\beta = [^{7}Li/^{6}Li_{std,raw}]/[^{7}Li/^{6}Li_{std,true}]$$

$$\alpha = [^{7}Li/^{6}Li_{spl,raw}]/[^{7}Li/^{6}Li_{spl,true}]$$

The relationship of the sample to standard $^{7}Li/^{6}Li$ isotope ratio derived from the raw SIMS data is therefore given by:

$$[^{7}Li/^{6}Li_{spl,true}]/[^{7}Li/^{6}Li_{std,true}] = \{[^{7}Li/^{6}Li_{spl,\,raw}]/[^{7}Li/^{6}Li_{std,raw}]\}*\{\beta/\alpha\} \quad (1)$$

and the corresponding δ^{7}Li by:

$$\delta^{7}Li_{spl,\,true,\,LSVEC} = 1000*\{([^{7}Li/^{6}Li_{spl,raw}]/[^{7}Li/^{6}Li_{std,raw}])*(\beta/\alpha)-1\} + \delta^{7}Li_{std,\,true,\,LSVEC} \quad (2)$$

The increase in α and β with decreasing Fo content of olivine is apparent from Fig. 2 in which the equivalent IMF in δ notation is plotted. Determining the relationship between α and composition requires normalization of $^{7}Li/^{6}Li_{spl,\,raw}$ to a constant value of $^{7}Li/^{6}Li_{std,raw}$ in order to account for instrument drift. For convenience we choose to normalize to $^{7}Li/^{6}Li_{std,true}$. This is done by either of two equivalent methods:

$$^{7}Li/^{6}Li_{spl,\,cor} = [^{7}Li/^{6}Li_{std,true}]*[^{7}Li/^{6}Li_{spl,\,raw}]/[^{7}Li/^{6}Li_{std,raw}] = [^{7}Li/^{6}Li_{spl,\,raw}]/\beta \quad (3)$$

or

$$^{7}Li/^{6}Li_{spl,cor} = 12.1729*(((1000*\{[^{7}Li/^{6}Li_{spl,\,raw}]/[^{7}Li/^{6}Li_{std,raw}]-1\} + \delta^{7}Li_{std,\,true})/1000) + 1)$$

The matrix effect is then obtained by linear regression of the α_{cor} and composition data, where $\alpha_{cor} = {}^{7}Li/^{6}Li_{spl,\,cor}/{}^{7}Li/^{6}Li_{spl,\,true}$, giving:

$$\alpha_{cor} = (1.116 \pm 0.0089) - (0.00128 \pm 0.00010)*Fo \qquad r^2 = 0.95 \quad (4)$$

and

$$\alpha_{cor} = (0.987 \pm 0.0014) + (0.00144 \pm 0.00011)*(\text{wt.\% FeO}) \qquad r^2 = 0.95 \quad (5)$$

In these equations Fo is expressed in mole percent and FeO in weight percent. Instrumental $^{7}Li/^{6}Li$ is typically fractionated by up to 30‰ from true values, so these absolute values for α_{cor} differ substantially from the actual instrumental fractionation. However, the important parameter is the slope of the compositional dependence, rather than the absolute value of α-provided a consistent procedure is used to apply the correction to both α and β. Error introduced by normalization is at least an order of magnitude smaller than the experimental uncertainties.

The matrix correction can also be approximated directly in terms of δ^{7}Li expressed in ‰:

$$\delta^{7}Li_{spl,\,true} = \left(\delta^{7}Li_{spl,\,raw} - IMF_{spl}\right) - \left(\delta^{7}Li_{std,\,raw} - IMF_{std}\right) + \delta^{7}Li_{std,\,true} \quad (6)$$

For analyses relative to KBH-1, regression of the sample average data from Table 2 gives

$$\text{IMF} = (118.2 \pm 9.1) - (1.30 \pm 0.10)*Fo \qquad r^2 = 0.95 \quad (7)$$

$$\text{IMF} = (1.46 \pm 0.12)*\text{FeO} - (13.0 \pm 1.6) \qquad r^2 = 0.95 \quad (8)$$

Eq. (6) is intrinsically normalized to the true standard value and is therefore a simpler procedure. Substituting Eqs. (7) and (8) into Eq. (6) and simplifying gives general equations that are independent of the specific standard used:

$$\delta^{7}Li_{spl,\,true} = \delta^{7}Li_{spl,\,raw} - \delta^{7}Li_{std,\,raw} + \delta^{7}Li_{std,\,true} + 1.30*\left(Fo_{spl} - Fo_{std}\right) \quad (9)$$

$$\delta^{7}Li_{spl,\,true} = \delta^{7}Li_{spl,\,raw} - \delta^{7}Li_{std,\,raw} + \delta^{7}Li_{std,\,true} - 1.46*\left(FeO_{spl} - FeO_{std}\right) \quad (10)$$

Eq. (9) is applicable only to olivine. Eq. (10) may be applicable to other phases, especially those consisting only (or mainly) of Fe, Mg and Si

Table 3
Li isotope results for Ko'olau olivines and pyroxenes

Sample	Spot	FeO wt.%	σ	Mg#	σ	$^{7}Li/^{6}Li$ sample	σ_{mean}	$^{7}Li/^{6}Li$ std	σ	$\delta^{7}Li$ uncor	σ	$\delta^{7}Li$ cor	σ
Olivine													
KOO17A-1	6f-1	13.3	0.1	86.1	0.1	12.4706	0.0058	12.4004	0.0122	9.1	1.1	3.4	1.1
KOO17A-1	6f-2	13.3	0.1	86.1	0.1	12.4654	0.0052	12.4004	0.0122	8.6	1.1	3.0	1.1
KOO17A-1	6f-3	13.3	0.1	86.1	0.1	12.4754	0.0055	12.4004	0.0122	9.4	1.1	3.8	1.1
KOO17A-1	6f-4	13.3	0.1	86.1	0.1	12.4552	0.0053	12.4004	0.0122	7.8	1.1	2.2	1.1
KOO17A-1 Ave	*4*	*13.3*	*0.3*	*86.1*	*0.3*					*8.7*	*0.7*	*3.1*	*0.7*
KOO17A-2	3f-1	12.9	0.1	86.5	0.1	12.5005	0.0091	12.4298	0.0110	9.1	1.2	3.9	1.2
KOO17A-2	6f-1	12.9	0.1	86.5	0.1	12.4793	0.0052	12.4004	0.0122	9.8	1.1	4.6	1.1
KOO17A-2	6f-2	12.9	0.1	86.5	0.1	12.4681	0.0063	12.4004	0.0122	8.9	1.1	3.7	1.1
KOO17A-2	6f-3	12.9	0.1	86.5	0.1	12.4757	0.0047	12.4004	0.0122	9.5	1.1	4.3	1.1
KOO17A-2 Ave	*4*	*12.9*	*0.1*	*86.5*	*0.2*					*9.3*	*0.4*	*4.1*	*0.4*
KOO17A-3	3f-1	13.8	0.1	85.6	0.1	12.4866	0.0102	12.4298	0.0110	8.0	1.2	1.7	1.2
KOO17A-3	3f-2	13.3	0.1	86.1	0.1	12.5130	0.0093	12.4298	0.0110	10.1	1.2	4.5	1.2
KOO17A-3	3f-3	12.3	0.1	87.1	0.1	12.5040	0.0081	12.4298	0.0110	9.4	1.1	5.0	1.1
KOO17A-3	3f-4	12.0	0.1	87.5	0.1	12.4778	0.0091	12.4298	0.0110	7.3	1.2	3.4	1.2
KOO17A-3	3f-5	11.7	0.1	87.8	0.1	12.4981	0.0110	12.4298	0.0110	8.9	1.3	5.5	1.3
KOO17A-3	3f-6	11.7	0.1	87.9	0.1	12.4839	0.0095	12.4298	0.0110	7.8	1.2	4.4	1.2
KOO17A-3	3f-7	11.6	0.1	87.9	0.1	12.4701	0.0099	12.4298	0.0110	6.6	1.2	3.3	1.2
KOO17A-3	3f-8	11.7	0.1	87.8	0.1	12.4835	0.0097	12.4298	0.0110	7.7	1.2	4.3	1.2
KOO17A-3	6f-1	13.0	0.3	86.4	0.3	12.4707	0.0051	12.4004	0.0122	9.1	1.2	3.8	1.1
KOO17A-3	6f-2	12.3	0.4	87.1	0.4	12.4616	0.0054	12.4004	0.0122	8.3	1.2	4.0	1.2
KOO17A-3	6f-3	12.0	0.2	87.5	0.2	12.4535	0.0060	12.4004	0.0122	7.7	1.2	3.9	1.1
KOO17A-3 Ave	*11*	*12.3*	*0.7*	*87.1*	*0.8*					*8.3*	*1.0*	*4.0*	*1.0*
KOO17A-4	6f-1	12.3	0.10	87.2	0.1	12.4307	0.0052	12.4004	0.0122	5.8	1.2	1.7	1.1
KOO17A-4	6f-2	11.6	0.10	87.9	0.1	12.4175	0.0053	12.4004	0.0122	4.8	1.2	1.4	1.1
KOO17A-4	6f-3	11.3	0.10	88.3	0.1	12.4243	0.0044	12.4004	0.0122	5.3	1.2	2.5	1.1
KOO17A-4	6f-4	11.2	0.10	88.4	0.1	12.4279	0.0058	12.4004	0.0122	5.6	1.2	2.9	1.1
KOO17A-4 Ave	*4*	*11.6*	*0.5*	*87.9*	*0.5*					*5.4*	*0.5*	*2.1*	*0.7*
KOO30A-1	6f-1	16.4	0.1	82.5	0.1	12.5255	0.0063	12.4004	0.0122	13.5	1.1	3.3	1.1
KOO30A-1	6f-2	16.4	0.1	82.5	0.1	12.5117	0.0052	12.4004	0.0122	12.4	1.1	2.2	1.1
KOO30A-1	6f-3	16.4	0.1	82.5	0.1	12.5313	0.0054	12.4004	0.0122	14.0	1.1	3.8	1.1
KOO30A-1 Ave	*3*	*16.4*	*0.31*	*82.5*	*0.4*					*13.3*	*0.8*	*3.1*	*0.8*
KOO30A-2	6f-1	16.7	0.1	82.2	0.1	12.5683	0.0047	12.4004	0.0122	16.9	1.1	6.3	1.1
KOO30A-2	6f-2	16.7	0.1	82.2	0.1	12.5724	0.0059	12.4004	0.0122	17.3	1.1	6.6	1.1
KOO30A-2	6f-3	16.7	0.1	82.2	0.1	12.5787	0.0061	12.4004	0.0122	17.8	1.1	7.1	1.1
KOO30A-2 Ave	*3*	*16.7*	*0.15*	*82.2*	*0.1*					*17.3*	*0.4*	*6.7*	*0.4*
KOO30A-3	6f-1	11.4	0.10	88.3	0.1	12.4675	0.0055	12.4004	0.0122	8.8	1.1	5.9	1.1
KOO30A-3	6f-2	11.4	0.10	88.3	0.1	12.4673	0.0063	12.4004	0.0122	8.8	1.1	5.9	1.1
KOO30A-3	6f-3	11.4	0.10	88.3	0.1	12.4369	0.0060	12.4004	0.0122	6.3	1.1	3.5	1.1
KOO30A-3 Ave	*3*	*11.4*	*0.45*	*88.3*	*0.4*					*8.0*	*1.4*	*5.1*	*1.4*
KOO30A-4	6f-1	16.9	0.1	81.9	0.1	12.6043	0.0037	12.4483	0.0071	15.9	0.7	5.0	0.7
KOO30A-4	6f-2	16.8	0.1	82.0	0.1	12.5831	0.0041	12.4483	0.0071	14.2	0.7	3.4	0.7
KOO30A-4	6f-3	17.0	0.1	82.1	0.1	12.5932	0.0039	12.4483	0.0071	15.0	0.7	4.3	0.7
KOO30A-4	6f-4	16.9	0.1	81.8	0.1	12.5960	0.0043	12.4483	0.0071	15.3	0.7	4.2	0.7
KOO30A-4	6f-5	16.9	0.1	82.0	0.1	12.5623	0.0048	12.4004	0.0122	16.5	1.1	5.6	1.1
KOO30A-4	6f-6	16.9	0.1	82.0	0.1	12.5761	0.0049	12.4004	0.0122	17.6	1.1	6.7	1.1
KOO30A-4 Ave	*6*	*16.9*	*0.07*	*81.9*	*0.1*					*15.7*	*1.2*	*4.9*	*1.2*
KOO30A-5	6f-1	14.6	0.1	84.8	0.1	12.4992	0.0045	12.4483	0.0071	7.5	0.7	0.2	0.7
KOO30A-5	6f-2	14.7	0.1	84.4	0.1	12.5200	0.0048	12.4483	0.0071	9.2	0.7	1.4	0.7
KOO30A-5	6f-3	16.5	0.1	82.3	0.1	12.5323	0.0048	12.4483	0.0071	10.1	0.7	−0.3	0.7
KOO30A-5	6f-4	14.7	0.1	84.5	0.1	12.4991	0.0045	12.4483	0.0071	7.5	0.7	−0.1	0.7
KOO30A-5 Ave	*4*	*14.7*	*0.31*	*84.6*	*0.4*					*8.6*	*1.3*	*0.3*	*0.8*
KOO55-1	6f-1	16.9	0.1	82.6	0.1	12.5568	0.0063	12.4004	0.0122	16.0	1.1	5.9	1.1
KOO55-1	6f-2	16.1	0.1	82.1	0.1	12.5489	0.0057	12.4004	0.0122	15.4	1.1	4.6	1.1
KOO55-1	6f-3	16.5	0.1	82.2	0.1	12.5527	0.0044	12.4004	0.0122	15.7	1.1	5.1	1.1
KOO55-1 Ave	*3*	*16.5*	*0.4*	*82.3*	*0.3*					*15.7*	*0.3*	*5.2*	*0.6*
KOO55-3	3f-1	13.9	0.1	85.3	0.1	12.4445	0.0102	12.4298	0.0110	4.6	1.2	−2.0	1.2
KOO55-3	3f-2	11.4	0.1	88.1	0.1	12.4999	0.0087	12.4298	0.0110	9.0	1.1	5.9	1.1
KOO55-3	3f-3	12.5	0.1	86.8	0.1	12.4933	0.0126	12.4298	0.0110	8.5	1.4	3.9	1.3
KOO55-3	3f-4	12.5	0.1	86.8	0.1	12.4727	0.0094	12.4298	0.0110	6.9	1.2	2.2	1.2
KOO55-3	3f-5	12.5	0.1	86.8	0.1	12.4783	0.0099	12.4298	0.0110	7.3	1.2	2.7	1.2
KOO55-3	3f-6	12.5	0.1	86.8	0.1	12.4194	0.0106	12.4298	0.0110	2.6	1.2	−2.1	1.2
KOO55-3	6f-7	12.3	0.1	87.1	0.1	12.4696	0.0065	12.4004	0.0122	9.0	1.1	4.7	1.1
KOO55-3	6f-8	12.5	0.1	86.9	0.1	12.4835	0.0066	12.4004	0.0122	10.1	1.1	5.4	1.1
KOO55-3 Ave	*8*	*12.3*	*0.46*	*87.1*	*0.5*					*8.5*	*1.2*	*4.1*	*1.5*

(continued on next page)

Table 3 (*continued*)

Sample	Spot	FeO wt.%	σ	Mg#	σ	$^{7}Li/^{6}Li$ sample	σ_{mean}	$^{7}Li/^{6}Li$ std	σ	$\delta^{7}Li$ uncor	σ	$\delta^{7}Li$ cor	σ
Olivine													
KOO55-4	3f-1	11.5	0.10	88.2	0.1	12.5281	0.0125	12.4538	0.0162	9.4	1.7	6.4	1.6
KOO55-4	3f-2	11.5	0.10	88.2	0.1	12.5311	0.0098	12.4538	0.0162	9.6	1.5	6.7	1.5
KOO55-4	3f-3	11.5	0.10	88.2	0.1	12.4186	0.0105	12.4538	0.0162	0.6	1.6	−2.4	1.5
KOO55-4	3f-4	11.5	0.10	88.2	0.1	12.4749	0.0115	12.4538	0.0162	5.1	1.6	2.1	1.6
KOO55-4	6f-1	11.5	0.10	88.2	0.1	12.4674	0.0057	12.4004	0.0122	8.8	1.1	5.8	1.1
KOO55-4	6f-2	11.5		88.2	1.0	12.4860	0.0067	12.4004	0.0122	10.3	1.1	7.3	1.7
KOO55-4 Ave	*6*	*11.5*	*0.2*	*88.2*	*0.2*					*9.5*	*0.6*	*6.6*	*0.6*
KOO55-5	6f-1	11.3	0.1	84.8	0.2	12.5062	0.0049	12.4004	0.0122	11.9	1.1	4.7	1.1
KOO55-5	6f-2	11.2	0.1	84.8	0.2	12.4862	0.0050	12.4004	0.0122	10.3	1.1	3.1	1.1
KOO55-5	6f-3	11.3	0.1	84.8	0.2	12.5013	0.0057	12.4004	0.0122	11.5	1.1	4.3	1.1
KOO55-5	6f-4	11.2	0.1	84.8	0.2	12.5144	0.0068	12.4004	0.0122	12.6	1.1	5.3	1.2
KOO55-5 Ave	*4*	*14.5*	*0.23*	*84.8*	*0.2*					*11.6*	*1.0*	*4.3*	*0.9*
KOO49-1	6f-1	17.4	1.2	81.4	0.4	12.4706	0.0058	12.4004	0.0122	9.1	1.1	−2.5	1.2
KOO49-1	6f-2	14.4	0.5	84.8	0.6	12.4654	0.0052	12.4004	0.0122	8.6	1.1	1.4	1.3
KOO49-1 Ave	*2*	*15.9*	*2.1*	*83.1*	*2.4*					*8.9*	*0.3*	*−0.5*	*2.8*
KOO49-5	6f-1	14.0	0.3	85.5	0.4	12.4804	0.0040	12.4483	0.0071	6.0	0.7	−0.4	0.8
KOO49-5	6f-2	20.2	2.4	78.1	1.0	12.5404	0.0034	12.4483	0.0071	10.8	0.6	−4.9	1.4
KOO49-5	6f-3	15.3	0.7	84.0	0.6	12.4715	0.0040	12.4483	0.0071	5.3	0.7	−3.0	1.0
KOO49-5 Ave	*3*	*16.5*	*3.3*	*82.5*	*3.9*					*7.3*	*3.0*	*−2.8*	*2.3*
Orthopyroxene													
KOO49-2	6f-1	12.9	0.9	79.3	1.5	12.4676	0.0068	12.4004	0.0122	8.8	1.2	3.7	1.7
KOO49-2	6f-2	12.9	0.9	79.3	1.5	12.4839	0.0066	12.4004	0.0122	10.1	1.1	5.0	1.7
KOO49-2	6f-3	12.9	0.9	79.3	1.5	12.5144	0.0066	12.4004	0.0122	12.6	1.1	7.4	1.7
KOO49-2	6f-4	12.9	0.9	79.3	1.5	12.5239	0.0064	12.4004	0.0122	13.4	1.1	8.2	1.7
KOO49-2 Ave	*4*	*12.9*	0.9	*79.3*	*1.5*					*11.2*	*2.1*	*−3.0*	*2.1*
Clinopyroxene													
KOO49-3	3f-1	8.1	0.2	78.9	0.3	12.5115	0.0143	12.4298	0.0110	10.0	1.5	2.3	1.3
KOO49-3	3f-2	8.1	0.2	78.9	0.3	12.5132	0.0140	12.4298	0.0110	10.1	1.4	2.4	1.3
KOO49-3	3f-3	8.1	0.2	78.9	0.3	12.4989	0.0163	12.4298	0.0110	9.0	1.6	1.3	1.4
KOO49-3	3f-4	8.1	0.2	78.9	0.3	12.5175	0.0133	12.4298	0.0110	10.5	1.4	2.8	1.2
KOO49-3	3f-5	8.1	0.2	78.9	0.3	12.5281	0.0125	12.4538	0.0162	9.4	1.7	1.7	1.1
KOO49-3	3f-6	8.1	0.2	78.9	0.3	12.5311	0.0098	12.4538	0.0162	9.6	1.5	1.9	1.0
KOO49-3	3f-7	8.1	0.2	78.9	0.3	12.4186	0.0105	12.4538	0.0162	0.6	1.6	−7.0	1.0
KOO49-3	3f-8	8.1	0.2	78.9	0.3	12.4749	0.0115	12.4538	0.0162	5.1	1.6	−2.6	1.1
KOO49-3	6f-1	8.1	0.2	78.9	0.3	12.5239	0.0068	12.4483	0.0071	9.5	0.8	1.8	0.8
KOO49-3	6f-2	8.1	0.2	78.9	0.3	12.5239	0.0068	12.4004	0.0122	13.4	1.1	5.6	0.8
KOO49-3	6f-3	8.1	0.2	78.9	0.3	12.4870	0.0058	12.4004	0.0122	10.4	1.1	2.7	0.7
KOO49-3 Ave	*11*	*8.1*	*0.2*	*78.9*	*0.3*					*10.2*	*1.3*	*2.5*	*1.3*
All	**# grains**					**Li ppm soln**[a]	**σ**	**$\delta^{7}Li$ soln**[a]	**σ**				
KOO17A Ave	4	12.5	0.8	87.0	0.8	2.01		4.98	0.50	8.0	1.5	3.3	0.9
KOO30A Ave	5	15.5	2.0	83.5	2.3	2.57		2.57	0.50	12.9	3.9	4.0	2.4
KOO49 ol Ave	2	16.3	2.6	82.8	3.0	2.32		2.31	0.74	7.9	2.3	−1.6	1.6
KOO49 all Ave	4							2.31	0.74			1.0	3.8
KOO55 Ave	4	12.7	1.8	86.3	2.1	2.06		4.63	0.50	9.3	4.0	5.1	1.1

$\delta^{7}Li$ values in ‰ relative to LSVEC.

[a] Li concentrations and $\delta^{7}Li$ values for bulk separates from Chan and Frey (2003).

(such as orthopyroxene), but this requires further investigation. We have tested the application of Eq. (10) in Section 5 to correct raw data on orthopyroxene from the Ko'olau basalts.

4.2. Deviations from linearity at high Fe contents

The above correction procedure is applicable only to the range of compositions listed above with the additional proviso that instrumental conditions are similar to those used on the ASU IMS-6f. A similar calibration performed on the IMS-3f shows a very similar linearity with an indistinguishable slope for all but the most Fe-rich (Fo74) sample (Fig. 3). On the other hand, data acquired for the Fo52 olivine (MHK-1) on the IMS-6f shows a major departure from linearity (Fig. 3). This departure from linearity was also indicated by SIMS data from the Allende meteorite (Channon et al., 2007) in which their Fig. 2 shows a systematic departure from expected chondritic $\delta^{7}Li$ for olivines<Fo73, the departure increasing with increasing Fe content. The non-linearity implies that further work is required before accurate $^{7}Li/^{6}Li$ ratios can be acquired for Fe-rich olivine using SIMS.

Similar behavior has been observed for the matrix-dependent fractionation of oxygen isotopes in olivine (Hervig et al., 1992; Eiler et al., 1997). In the case of oxygen isotopes, a linear relationship between IMF and Fe content exists from Fo100–~Fo80. It seems reasonable to assume that the linearity also holds for Li isotopes for compositions poorer in Fe than those investigated here, i.e. from Fo94–Fo100, but this requires verification. The non-linear behavior shown by the IMS-3f for the Fo74 olivine suggests that instrumental conditions play an important role. A major difference between these two instruments is the accelerating voltage: 4.5 kV (3f) and 10 kV (6f).

4.3. Implications for SIMS analysis

The strong matrix effect of 1.3‰ per Fo unit (1.46‰ per wt.% FeO) for magnesian olivine illustrates the importance that should be placed on evaluating such effects in isotope analysis by SIMS. A lack of

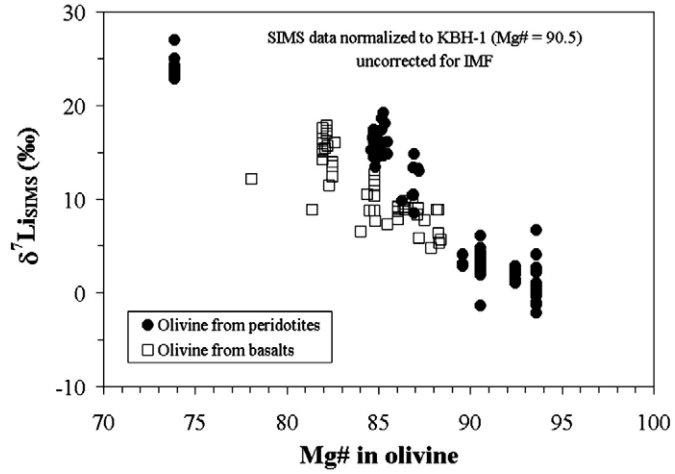

Fig. 1. Uncorrected δ^7Li values determined by SIMS (IMS-6f) for samples with Mg#>70 used in this study, showing the correlation of Li isotope composition with olivine composition in this range. The δ^7Li was calculated as $1000*\{([^7Li/^6Li_{spl,\ raw}]/[^7Li/^6Li_{KBH1,raw}])-1\}+3.4$.

systematic investigation combined with some fortuitous sample choice has led many previous studies to suggest that matrix effects are minor. In most cases it appears that such conclusions were justified for large-scale effects, but it has never been clear how much the details are being affected, in particular with regard to systematic bias. However, as additional data accumulated the probability of matrix effects playing a role has become increasingly apparent (Kasemann et al., 2005; Jeffcoate et al., 2007). As discussed above, the absolute fractionation of ^{7}Li/^{6}Li by the SIMS can be large (in the present study up to ~50‰). With the necessary sample-standard bracketing, the matrix effect becomes an issue of the difference between sample and standard composition, as shown by Eq. (10). Because olivine exhibits a large difference in mean atomic mass between end-members of the solid solution series compared with other common rock-forming silicates, there is some reason to believe that olivine matrix effects are larger than for other minerals or between minerals and basaltic glasses (Steele et al., 1981; Hervig et al., 2002). Nevertheless, until some understanding of the physics is reached, or the effects are empirically quantified in a wide range of compositions, the effects of matrix on Li contents and Li isotope ratio analysis must be regarded as a major source of uncertainty, and compositional differences between samples and standards best kept to a minimum. The consideration of matrix effects is especially recommended where inter-mineral isotopic equilibrium is being assessed, or where quantitative interpretations of isotope profiles in compositionally zoned minerals are desired. An illustration of the latter follows in the next section.

Application of a matrix effect correction introduces additional formal uncertainty to the analysis of δ^7Li by SIMS, despite the substantial improvement in accuracy. As discussed above, the uncertainty is magnified by the difference in composition between sample and standard. From Eqs. (7) and (9), the uncertainty in the slope of the calibration adds an uncertainty of 0.1‰ for every Fo unit difference between sample and standard composition. Considering typical analytical conditions where 1σ counting statistics errors on both sample and standard are 0.7‰, the added uncertainty in the compositional dependence produces total 1σ uncertainty in absolute accuracy ranging from 1 to 2‰ for the range of magnesian olivine standard compositions investigated here. Because we have not characterized the departure from linearity in any quantitative detail, Li isotope analysis in more Fe-rich olivines is substantially more uncertain, and awaits further calibration work. Relative differences in δ^7Li between analyses of materials of homogeneous composition are, of course, determined with substantially greater precision.

5. Results for Ko'olau basalt phenocrysts

Table 3 lists the SIMS Li isotope data for the Ko'olau phenocrysts samples as well as bulk analyses from Chan and Frey (2003). These samples were acquired with the intention of using them in the matrix correction scheme, but both δ^7Li and Fo content were found to vary among grains from a single sample, and within individual grains, and one separate contained significant quantities of pyroxene. This problem prevented their use as a primary standard for calibration of the matrix effects. There is a broad increase in raw δ^7Li with

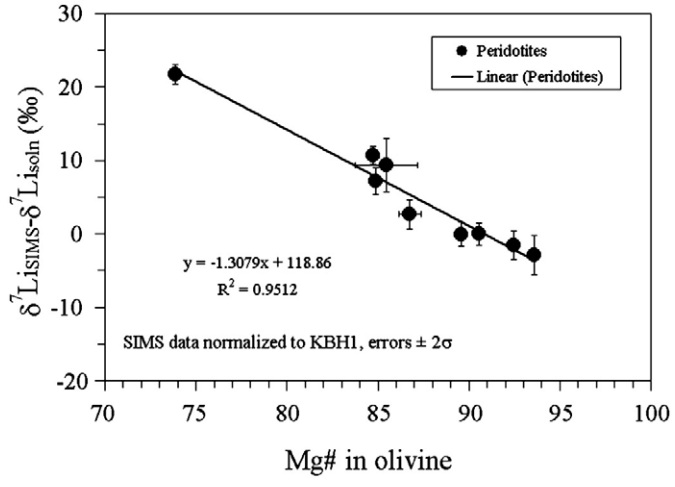

Fig. 2. Magnitude of the IMF as a function of olivine composition for Mg-rich olivines, determined on the IMS-6f SIMS at ASU. The IMF is calculated as the difference between the average δ^7Li measured by SIMS on a collection of grains and that determined by either TIMS or MC-ICP-MS after dissolution and chromatographic purification of a bulk olivine separate. Each symbol represents the mean of between 5 and 15 SIMS analyses. Errors are propagated from both solution and SIMS analyses, and represent ±2 standard deviations of the population of measurements (i.e., they are not based on instrumental counting statistics). The line and its equation represent a standard *y* on *x* linear regression.

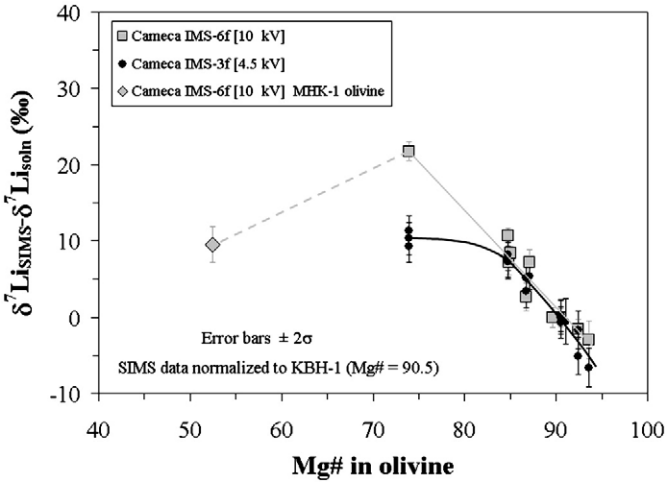

Fig. 3. Magnitude of the IMF as a function of olivine composition, including IMS-6f data from an Fe-rich olivine and IMS-3f data for the samples shown in Fig. 2. The solid gray line is the linear fit to the IMS-6f data for Mg-rich olivines (gray squares) from Fig. 2. The dashed gray line shows departure from this line implied by the Fe-rich olivine sample MHK-1 (gray diamond, mean ±2σ of twelve SIMS analyses on multiple grains and two MC-ICP-MS analyses of a single separate). The solid black line is fitted by eye to the IMS-3f data on Mg-rich olivines (solid black circles). These data show departure from a linear matrix effect for olivines with Mg#<~74 (IMS-6f) and Mg#<~85 (IMS-3f).

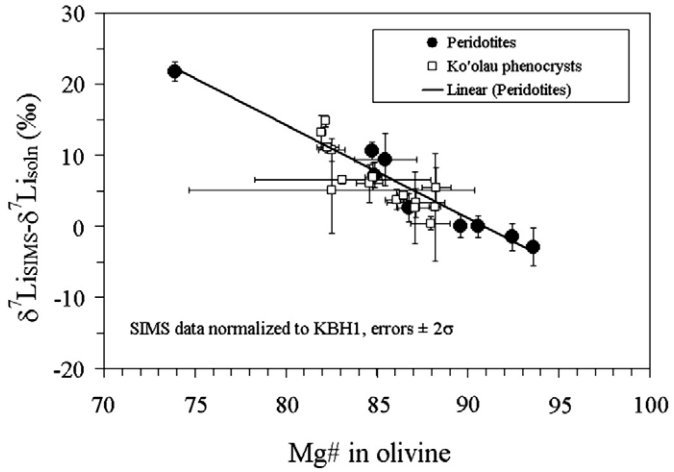

Fig. 4. Magnitude of the IMF (IMS-6f) of Li isotope composition as a function of olivine composition for Hawaiian olivine phenocrysts compared with Mg-rich olivines from Fig. 2. Each square symbol is the average composition of a single olivine grain and the error bars represent ± two standard deviations in the range of values measured. The error bars therefore indicate sample heterogeneity rather than analytical uncertainty.

decreasing Fo content in the Hawai'i olivines (Fig. 1), but also in the difference between the raw δ^7Li and δ^7Li of the bulk separate determined by TIMS (Fig. 4). This latter correlation corresponds closely to that defined by the mantle olivine standards and is due primarily to the matrix effect discussed above, providing independent confirmation of the general accuracy of the matrix correction.

Figs. 5 and 6 illustrate the matrix-corrected δ^7Li variation as a function of Mg# and Li content of the olivines, respectively. For the clinopyroxene in KOO-45, the raw ^{7}Li/^{6}Li ratios were ratioed to BHVO-2G, using the relationship between KBH1 and BHVO-2G reported in the footnote to Table 2. For the orthopyroxene, the raw ^{7}Li/^{6}Li ratios were corrected using Eq. (10), i.e. based on the wt.% FeO content.

As suggested by Fig. 3, the spread in δ^7Li is much reduced by matrix correction, and most of the data define a relatively narrow spread around the bulk analyses from Chan and Frey (2003), with δ^7Li values of individual grains both above and below the bulk δ^7Li value. However, there appears to be a systematic bias in the SIMS Li abundance measurements, which for three of the four samples appear significantly lower than the TIMS concentrations. Preliminary data from our laboratory suggest a systematic matrix effect in Li abundance measurements of olivine as a function of Fe content (see Section 3.3 and Fig. A1). The smallest discrepancy between SIMS and TIMS abundances is for KOO17, the sample closest in composition to the KBH1 standard.

Despite the approximate correspondence of average δ^7Li values, some individual analyses or groups of analyses deviate significantly and provide insights into the ability of magmatic phenocrysts to record faithfully the δ^7Li of the melt from which they were crystallized. No correlation between δ^7Li and Mg# is expected to arise from high temperature magmatic fractionation during fractional crystallization (Tomascak et al., 1999). In general, there is a poor correlation of δ^7Li with Mg#, which is to be expected if variations in δ^7Li reflect late stage and/or post-magmatic processes. Li isotopes are especially prone to such disturbance because of high Li diffusivity and the capacity for Li diffusion to cause isotope fractionation (Giletti and Shanahan, 1997; Richter et al., 2003; Coogan et al., 2005; Lundstrom et al., 2005; Singletary and Bell, 2007). Although only four or five crystals were analyzed per sample, the data suggest differences in the degree of homogeneity between samples. KOO17A is relatively homogeneous, and has an average δ^7Li and Li content close to that of the bulk separate. The other samples are less homogeneous.

Sample KOO30A is noteworthy because each olivine phenocryst has a distinct Li content and δ^7Li value. This heterogeneity could have been produced if different phenocryst populations were mixed, but Li diffusion should have rapidly erased such differences. Another possibility is that these phenocrysts represent a chemical gradient in the matrix of the rock sampled. Such a gradient could be produced by Li escape from the surface of a lava flow, or some form of fluid–rock interaction after the magma solidified, but before Li ceased to diffuse. There is a hint that lower Li contents are correlated with lighter isotope ratios in this sample. Such a correlation would preclude

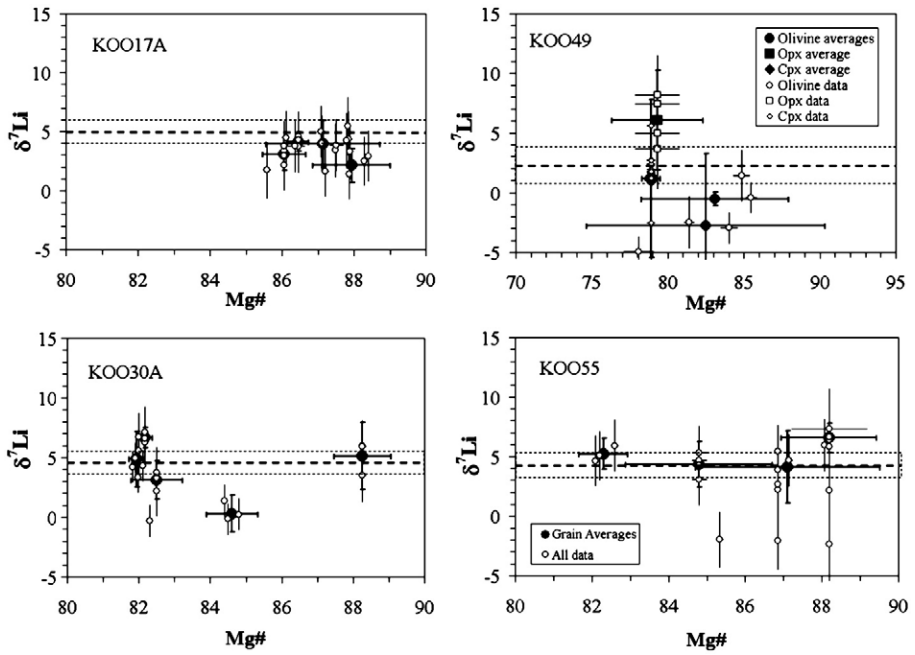

Fig. 5. Matrix-corrected δ^7Li vs. Mg# in olivine for olivine phenocryst separates from four Ko'olau basalt samples. Sample KOO49 also includes data from orthopyroxene and clinopyroxene grains in the separate. Solid symbols represent the mean and ±2σ range for each grain, and include data from both IMS-3f and IMS-6f. Open symbols represent individual SIMS analyses and their associated 2σ standard errors derived from counting statistics. The dashed horizontal lines are the mean ± 2σ of the bulk olivine separate determined using TIMS by Chan and Frey (2003).

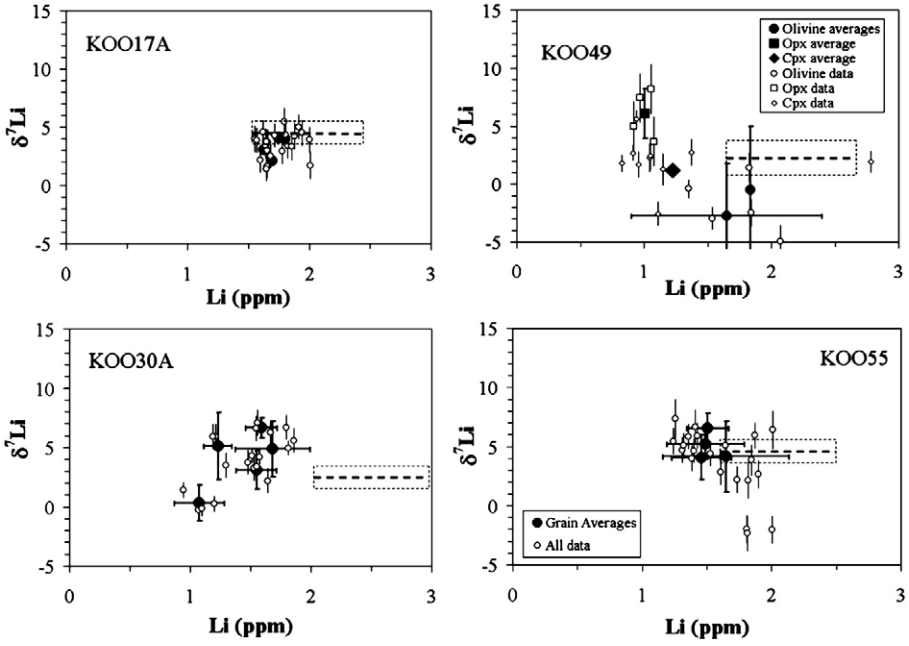

Fig. 6. Matrix-corrected δ^7Li vs. Li content of olivine for olivine phenocryst separates from four Ko'olau basalt samples. Sample KOO49 also includes data from orthopyroxene and clinopyroxene grains in the separate. Solid symbols represent the mean and ±2σ range for each grain and include data from both IMS-3f and IMS-6f. Open symbols represent individual SIMS analyses and their associated 2σ standard errors derived from counting statistics. The dashed box represents ±2σ around the mean of the Li content and δ^7Li of the bulk olivine separate determined using TIMS by Chan and Frey (2003). We assigned an arbitrary uncertainty of ±1 ppm (2σ) to the Li abundance determination by TIMS.

diffusive fractionation as the cause of isotope variation, because preferential gain or loss of the lighter isotope is expected in this case.

Samples KOO49 and KOO55 both contain grains where portions or most of the grains have anomalously low δ^7Li values that are uncorrelated with other compositional variables. These may well be due to post-solidification disturbance. In KOO49 the olivine grains appear to be isotopically lighter than the pyroxene grains in the separate, which have corrected δ^7Li values closer to typical mantle values. It is notable that the orthopyroxene δ^7Li values, corrected on the basis of difference in FeO content from KBH1, are much closer to expected "mantle" values than the uncorrected values (Table 3). The clinopyroxene δ^7Li values, determined by referring raw ^{7}Li/^{6}Li to the BHVO-2G standard, are also mostly far closer to expected values than the clinopyroxene δ^7Li determined from the olivine-based matrix correction. This confirms previous results (Decitre et al., 2002; Kasemann et al., 2005) of limited matrix effect between clinopyroxene and basaltic glass, but suggests that orthopyroxene may depart from the basalt glass calibration. The δ^7Li difference between olivine and pyroxenes suggests that olivine is more susceptible to disturbance, perhaps because of higher Li diffusivity. Very low δ^7Li occurs at one end of a linear traverse across the clinopyroxene grain, which may be due to preferential diffusive gain of ^{6}Li at the grain margin. In general, it appears that various processes may alter the Li isotope composition of magmatic phenocrysts and compromise their capability to record primary magmatic isotope ratios.

Jeffcoate et al., 2007 recorded similar magnitudes of variability in Hawaiian olivine phenocrysts, although the effect of matrix composition on δ^7Li in these zoned olivines (and perhaps in pyroxenes) is a likely complicating factor. It is probable that systematic matrix effects occur in other ferromagnesian minerals, but we speculate that the effect in olivine is greater than for other common rock-forming minerals because of the high relative change in mean atomic mass.

In summary, the Li isotope data from the Ko'olau basalt phenocrysts show moderate isotopic variability, greater than could be expected due to equilibrium fractionation processes at high temperature. These variations suggest that Li isotopes are easily disturbed in young basalts, at least on a local scale, with diffusive fractionation of Li isotopes likely playing a significant role. We concur with Jeffcoate et al., 2007 that caution should be applied when inferring primary magmatic Li isotope compositions from either lavas or their separated phenocrysts. This propensity to disturbance limits, but does not preclude, the use of Li isotopes to trace crustal recycling in the mantle. As is the case with hydrogen and its isotopes, some additional work may be necessary to assess the degree of disturbance before this method can be applied with confidence to problems where the detection of small magnitude variations in isotope composition shifts is required. On the other hand, this work confirms the potential use of Li and its isotopes to trace volcanic processes, possibly to temperatures lower than accessible by other petrologic methods.

6. Summary

The composition of olivine strongly affects measurements of ^{7}Li/^{6}Li by SIMS. At high Mg/Fe ratios (74<Fo<100) the effect for the Cameca IMS-6f is a linear function of composition, amounting to a 1.3‰ increase in δ^7Li for each mole percent decrease in forsterite component. At Fo contents below this range (i.e., higher Fe contents) the compositional effect reaches a maximum and then decreases. This change to non-linear behavior occurs at lower Fe contents (~Fo80) on the IMS-3f and is suggested to be a function of accelerating potential differences between the two SIMS instruments. Analysis of a series of olivine phenocrysts demonstrates the importance of correcting for matrix effects in the analysis of zoned crystals, which has important implications for applications to magmatic evolution of volatiles and cooling histories derived from Li and δ^7Li zoning profiles. However, after correction of these matrix effects, deviations from magmatic values are still apparent in phenocrysts from Hawaiian lavas, suggesting late stage modification of Li isotopes during and immediately after eruption, as inferred by other workers. These late-stage variations may compromise the use of Li isotopes in tracer studies.

Acknowledgments

We acknowledge the diverse and invaluable contributions to Li isotope geochemistry of our late colleague Lui Chan, who also provided the olivine separates from Hawai'i used in this study.

Roberta Rudnick hosted and supervised the MC-ICP-MS Li isotope analyses at the University of Maryland and her comments and participation in stimulating discussions are much appreciated. We are also grateful to Michael Seitz and David L. Reid for contributing samples to this study. Yunbin Guan provided valuable technical assistance with the IMS-6f and Gordon Moore assisted with electron microprobe analysis. We acknowledge the assistance of Melanie Channon and Kimberley Genareau in performing some of the analyses reported herein. Thorough reviews by Simone Kasemann and an anonymous reviewer improved the manuscript. The work was supported by grants from the National Science Foundation (EAR-0538320) and NASA (NNG06GF08G).

Appendix A. Supplementary data

Supplementary data associated with this article can be found, in the online version, at doi:10.1016/j.chemgeo.2008.10.008.

References

Armstrong, J.T., 1988. Quantitative analysis of silicate and oxide materials: comparison of Monte Carlo, ZAF and $\phi(\rho z)$ procedures. In: Newbury, D.E. (Ed.), Microbeam Analysis 1988. San Francisco Press, pp. 239–246.

Aulbach, S.A., Rudnick, R.L., McDonough, W.F., 2008. Li–Sr–Nd isotope signatures of the plume and cratonic lithospheric mantle beneath the margin of the rifted Tanzanian craton (Labait). Contrib. Mineral. Petrol. 155, 79–92.

Beck, P., Barrat, J.A., Chaussidon, M., Gillet, P., Bohn, M., 2004. Li isotopic variations in single pyroxenes from the Northwest Africa 480 shergottite (NWA480): a record of degassing of Martian magmas. Geochim. Cosmochim. Acta 68, 2925–2933.

Beck, P., Chaussidon, M., Barrat, J.A., Gillet, P., Bohn, P., 2006. Diffusion induced Li isotopic fractionation during the cooling of magmatic rocks: the case of pyroxene phenocrysts from nakhlite meteorites. Geochim. Cosmochim. Acta 70, 4813–4825.

Bell, D.R., Rossman, G.R., 1992. Water in the Earth's mantle: the role of nominally anhydrous minerals. Science 255, 1391–1397.

Bevington, P., Robinson, D.K., 2002. Data Reduction and Error Analysis for the Physical Sciences. McGraw-Hill, New York. 336 pp.

Chan, L.H., Frey, F.A., 2003. Lithium isotope geochemistry of the Hawaiian plume: results from the Hawaii Scientific Drilling Project and Koolau volcano. Geochem. Geophys. Geosyst. 4, 8707.

Channon, M., Bell, D.R., Hervig, R.L., and Buseck, P.R. 2007 Isotopic composition of lithium in the Allende meteorite. Lunar and Planetary Science Conference 38, p. 1877.pdf. Lunar and Planetary Institute, Houston, TX.

Coogan, L.A., Kasemann, S.A., Chakraborty, S., 2005. Rates of hydrothermal cooling of new oceanic upper crust derived from lithium-geospeedometry. Earth Planet. Sci. Lett. 240, 415–424.

Decitre, S., Deloule, E., Reisberg, L., James, R.H., Agrinier, P., Mevel, C., 2002. Behavior of Li and its isotopes during serpentinization of oceanic peridotites. Geochem. Geophys. Geosyst. 3 (1). doi:10.1029/2001GC000178.

Doyle, P.M. 1999. A petrologic and geochemical study of the megacryst suite and related nodules from the Gansfontein kimberlite, RSA. Unpubl. B.S.c.(Hons.) thesis, Univ. Cape Town, 132 pp.

Eiler, J., Graham, C.M., Valley, J.W., 1997. SIMS analysis of oxygen isotopes; matrix effects in complex minerals and glasses. Chem. Geol. 138, 221–244.

Giletti, B.J., Shanahan, T.M., 1997. Alkali diffusion in plagioclase feldspar. Chem. Geol. 139, 3–20.

Hervig, R.L., Williams, P., Thomas, R.M., Schauer, S.N., Steele, I.M., 1992. Microanalysis of oxygen isotopes in insulators by secondary ion mass spectrometry. Int. J. Mass Spectrom. Ion Process. 120, 45–63.

Hervig, R.L., Bell, D.R., Moore, G., Williams, L.B., Yamamoto, J., Buseck, P.R., 2004. SIMS analyses for Li isotope ratios: from olivine to clay minerals. Eos Trans. AGU, 85 (47), Fall Meet. Suppl., Abstract V51C-0593.

Jeffcoate, A., Elliott, T., Kasemann, S., Ionov, D., Cooper, K., Brooker, R., 2007. Li isotope fractionation in peridotites and mafic melts. Geochim. Cosmochim. Acta 71, 202–218.

Kasemann, S., Jeffcoate, A.B., Elliott, T., 2005. Lithium isotope composition of basalt glass reference material. Anal. Chem. 77, 5251–5257.

Lee, C.-T., Rudnick, R.L., 1999. Compositionally stratified cratonic lithosphere: petrology and geochemistry of peridotite xenoliths from the Labait volcano, Tanzania. In: Gurney, J., Gurney, J., Pascoe, M., Richardson, S. (Eds.), The P. H. Nixon Volume. Proceedings of the 7th International Kimberlite Conference, vol. 2. Red Roof Design, Cape Town, pp. 503–521.

Lundstrom, C.C., Chaussidon, M., Hsui, A.T., Kelemen, P.B., Zimmerman, M., 2005. Observations of Li isotopic variations in the Trinity ophiolite: evidence for isotopic fractionation by diffusion during mantle melting. Geochim. Cosmochim. Acta 69, 735–751.

Qi, H.P., Taylor, P.D.P., Berglund, M., DeBievre, P., 1997. Calibrated measurements of the isotopic composition and atomic weight of the natural Li isotopic reference material IRMM-016. Int. J. Mass Spectr. Ion Process. 171, 263–268.

Richter, F.M., Davis, A.M., De Paolo, D.J., Watson, E.B., 2003. Isotope fractionation by chemical diffusion between molten basalt and rhyolite. Geochim. Cosmochim. Acta 67, 3905–3923.

Rudnick, R.L., McDonough, W.F., Orpin, A., 1994. Northern Tanzanian peridotite xenoliths: a comparison with Kaapvaal peridotites and inferences on metasomatic interactions. In: Meyer, H.O.A., Leonardos, O. (Eds.), Kimberlites, Related Rocks and Mantle Xenoliths, Vol. 1. Proc. 5th Internat. Kimberlite Conf. C.P.R.M., Brasilia, pp. 336–353.

Scoon, R.N., Mitchell, A.A., 2004. The platiniferous dunite pipes in the eastern limb of the Bushveld Complex: review and comparison with unmineralized discordant ultramafic bodies. S. Afr. J. Geol. 107, 505–520.

Seitz, H.-M., Brey, G.P., Lahaye, Y., Durali, S., Weyer, S., 2004. Lithium isotopic signatures of peridotite xenoliths and isotopic fractionation at high temperature between olivine and pyroxenes. Chem. Geol. 212, 163–177.

Seitz, H.M., Woodland, A.B., 2000. The distribution of lithium in peridotitic and pyroxenitic mantle lithologies — an indicator of magmatic and metasomatic processes. Chem. Geol. 166, 47–64.

Singletary, S.J., Bell, D.R., 2007. Bulk diffusion and isotopic fractionation of lithium in olivine: an experimental study. Eos Trans. AGU 88 (52) Abstract V51E-0838.

Steele, I.M., Hervig, R.L., Hutcheon, I.D., Smith, J.V., 1981. Ion microprobe techniques and analyses of olivine and low-Ca pyroxene. Am. Mineral. 66, 526–546.

Tomascak, P.B., Tera, F., Helz, R.T., Walker, R.J., 1999. The absence of lithium isotope fractionation during basalt differentiation: new measurements by multicollector sector ICP-MS. Geochim. Cosmochim. Acta 63, 907–910.